Pacific Northwest
NATIONAL LABORATORY

PNNL-36655

Corrosion of SS 316, Inconel 617, Inconel 625 in molten chloride salt with emphasis on the speciation of Cr, Ni, and Co in molten salt matrix by XAFS

September 2024

Thomas Hartmann
Tatiana Levitskaia
Daria Boglaienko
Daniel Koury

U.S. DEPARTMENT OF ENERGY

Prepared for the U.S. Department of Energy
under Contract DE-AC05-76RL01830

DISCLAIMER

PACIFIC NORTHWEST NATIONAL LABORATORY
operated by
BATTELLE
for the
UNITED STATES DEPARTMENT OF ENERGY
under Contract DE-AC05-76RL01830

Printed in the United States of America

Available to DOE and DOE contractors from
the Office of Scientific and Technical Information,
P.O. Box 62, Oak Ridge, TN 37831-0062
www.osti.gov
ph: (865) 576-8401
fox: (865) 576-5728
email: reports@osti.gov

Available to the public from the National Technical Information Service
5301 Shawnee Rd., Alexandria, VA 22312
ph: (800) 553-NTIS (6847)
or (703) 605-6000
email: info@ntis.gov
Online ordering: http://www.ntis.gov

PNNL-36655

Corrosion of SS 316, Inconel 617, Inconel 625 in molten chloride salt with emphasis on the speciation of Cr, Ni, and Co in molten salt matrix by XAFS

A study in support of MSR technology

September 2024

Thomas Hartmann
Tatiana Levitskaia
Daria Boglaienko
Daniel Koury

Prepared for
the U.S. Department of Energy
under Contract DE-AC05-76RL01830

Pacific Northwest National Laboratory
Richland, Washington 99354

Abstract

The corrosion behavior of materials used in the construction and operation of molten salt reactors is of great interest to the molten salt reactor (MSR) community, and besides the significant efforts in the past on low chromium nickel-based alloys such as Hastelloy N (Alloy N), a dedicated ASME coded MSR structural material for MSR deployment is not available. In the present study we intent to decipher the very elemental phenomena on the corrosion of austenitic chromium-containing stainless steel SS316, as well as Inconel 625 and ASME-coded high temperature Alloy (Inconel) 617. At this, our goal was to investigate diffusivity of alloying metals such as chromium, iron, nickel, and cobalt (if applicable) at the molten salt alloy interface, and further determined the speciation of the corrosion products by x-ray absorption spectroscopy. In this study we have selected the binary surrogate salt NaCl-$MgCl_2$ as test matrix at temperatures of 550 °C and 650 °C. The materials as tested aren't by any means prospective candidate materials for MSR application due to their high chromium content and the derived high corrosion rates in contact with molten chloride salts. Their use here, however, is valuable to gain a fundamental understanding on diffusivity and speciation formation under pseudo *in-operando* conditions of MSRs.

We initiated and are in continuation of conducting ampoule type corrosion testing at 550 °C and 650 °C to determine chromium diffusivity and the related activation energy as well as the speciation of the corrosion products. Corrosion rates along the alloy-molten salt interface will be determined through the solution of second Fick's law using the Boltzmann-Matano method and an error-function type simplification. Therefore, accurate semi-quantitative elemental analysis by SEM-EDS ($\pm$ 0.2 wt.-%, $\pm$ 1 μm) will be used to determine diffusivity and overall corrosion rates. We have successfully performed a proof-of-concept experiment showing that x-ray absorption spectroscopy (XAS) on corroded metal foils can be applied to determine the speciation of MSR corrosion products (metal chlorides) in a rather novel approach. At this, speciation of metal chlorides has been determined on corroded foils of SS316 and IN625, while data for IN617 are expected for FY 2025.

Summary

The aim of this research is to determine the corrosion behavior of alloying metals in SS316, IN 625, and IN 617 in contact with an eutectic molten NaCl-$MgCl_2$ salt matrix at 550 °C and 650 °C, and to provide information on the speciation of corrosion products. In support of our experimental agenda, we have established a research partnership with the radiochemistry group at the University of Nevada, Las Vegas (UNLV). This collaboration became necessary to gain access to suitable laboratory space: such as inert glove-boxed, furnaces, electron microscopy and elemental analysis. We have established an adequate research environment to satisfy the proposed work-scope and to provide data on diffusivity, corrosion kinetics, activation energy, and product speciation as projected, however, with some delay. Hereby, the FY 2024 data will provide information using eutectic surrogate salt, while in FY 2025 we are planning to deploy near *in-operando* conditions using ternary Na-Mg-U chloride salt melts and eventually the addition of fission tellurium.

In this report we are providing extensive background information on (1) the thermodynamics and electrochemistry of corrosion in chloride salts, (2) the thermodynamics of the NaCl-$MgCl_2$ system in comparison with the Na-U-Cl system, (3) a review on Fe-Cr-Ni alloys, (4) the development of high-temperature alloys for nuclear deployment and specifically the metallurgy of alloy (Inconel) 617. We are further discussing the development of alloys suitable for MSR application as well as the constituency of high-temperature alloys and superalloys.

As a future MSR-compatible alloy, Haynes 244 is, on paper, a very promising candidate due to its low-chromium content and its superior high-temperature strength compared with Hastelloy N. Haynes 244 is an upgraded alloy over Alloy 242. Limited data suggests that Haynes 244 possesses better high-temperature capabilities, including creep strength, compared with Haynes 242. Alloy 244 is age-hardenable by formation of Ni_2(Cr,Mo,W) domains, which are structurally similar to the strengthening domains in alloy 242. However, corrosion data or data on its nuclear properties are not available to larger extent, and we will therefore study corrosion properties of Haynes 244 in FY 2025.

Acknowledgments

The research presented here was supported by the Molten Salt Reactor program of the DOE Office of Nuclear Energy. PNNL is a multi-program national laboratory operated for the U.S. Department of Energy (DOE) by Battelle Memorial Institute under Contract No. DE-AC05-76RL01830.

Acronyms and Abbreviations

ADTT	Accelerator-driven transmutation technology
Al	Aluminum
AMMT	Advanced materials & manufacturing technologies
APT	Atom probe tomography
As	Arsenic
ASME	American society of mechanical engineers
B	Boron
Bi	Bismuth
Bcc	Body-centered cubic
C	Carbon
Cu	Copper
Co	Cobalt
Cr	Chromium
DIN	German institute for standardization
DOE	Department of Energy
EDS	Energy-dispersive x-ray spectroscopy
F	Fluorine
Fcc	Face-centered cubic
Fe	Iron
GB	Grain-boundary
Gen-IV	Generation IV international forum
GPa	Gigapascal
HAADF	High angle annular darkfield imaging
Hcp	Hexagonal close packing
He	Helium
Hz	Hertz
IGC	Intergranular cracking
IN	Inconel
INL	Idaho National Laboratory
MCFR	Molten chloride fast reactor
MCSFR	Molten chloride salt fast reactor
$MgCl_2$	Magnesium chloride
Mo	Molybdenum
Mn	Manganese
NRC	Nuclear regulatory commission
MPa	Megapascal

MSR	Molten salt reactor
MSRE	Molten salt reactor experiment
MSRR	Molten Salt Research Reactor
NaCl	Sodium chloride
Nb	Niobium
Ni	Nickel
NRC	Nuclear regulatory commission
NTD	National technical director
nm	Nanometer
ORNL	Oak ridge national laboratory
Os	Osmium
P	Phosphor
PNNL	Pacific Northwest National Laboratory
UNS	Unified numbering system
Pt	Platinum
Re	Rhenium
S	Sulphur
SEM	Scanning electron microscopy
Si	Silicon
Ta	Tantalum
Te	Tellurium
TEM	Transmission electron microscopy
Ti	Titanium
UNLV	University of Nevada, Las Vegas
V	Vanadium
VdTÜV	Association of Technical Inspection Agencies
W	Tungsten
WDS	Wavelength dispersive x-ray spectroscopy
Wt.%	weight-percent
XAFS	X-ray absorption fine structure
XAS	X-ray absorption spectroscopy
XES	X-ray emission spectroscopy

Contents

Abstract iv
Summary v
Acknowledgments vi
Acronyms and Abbreviations vii
1.0 Introduction and background 1
1.1 Thermodynamic considerations 2
1.2 NaCl-$MgCl_2$ salt system 5
1.3 Alloy systems 7
1.4 Iron-chromium-nickel-based systems 8
1.5 Development of high-temperature alloys for nuclear applications 9
1.6 Metallurgy of Alloy 617 10
1.6.1 Solution strengthening and precipitation hardening of Alloy 617 10
1.6.2 Creep strength of Alloy 617and narrowing chemical bandwidth 12
1.6.3 Microstructure of Alloy 617 and Alloy 617B 13
1.6.4 Solid Solution strengthening of high temperature alloys 15
1.7 Suitable alloys for MSR application 18
1.8 Constituency and properties of high-temperature alloys and superalloys 23
1.8.1 Common nickel-based high-temperature alloys 25
1.8.2 Properties of nickel-based superalloys in comparison 29
1.8.3 High-temperature properties of nickel-based alloys and superalloys 31
1.8.4 High-temperature corrosion resistance Haynes and Inconel 35
2.0 Experimental 37
2.1 Sample Preparation 37
2.1.1 Fabrication of XAS specimen 37
2.1.2 Fabrication of diffusion specimen 37
2.2 Analysis 39
2.2.1 X-ray Absorption Spectroscopy (XAS) 39
2.2.2 Speciation of metal-chloride corrosion products 40
3.0 Outlook for FY2025 43
4.0 References 44

Figures

Figure 1. Redox potentials of various redox couples as a function of temperature in chloride salts. *Solid line*: metal dissolution at a_{Mn^+} of 1 μM/L. *Dotted* 4
Figure 2. The NaCl-$MgCl_2$ system: Calculated and experimental data [17] 5
Figure 3. NaCl-$MgCl_2$ system: Calculated activities in the liquid at 800 °C [17] 6
Figure 4. The Systems NaCl-UCl_3 and NaCl-UCl_4 [18] 6
Figure 5. Schematic representation of the isothermal section of the ternary Fe-Cr-Ni-based system [19]. 9
Figure 6. Time-temperature-transformation diagram of boron-modified Alloy 617B (Alloy 617mod) [24] 11
Figure 7. Creep rupture strength of Alloy 617 as a function of rupture time [22] 12
Figure 8. a) HAADF (high-angle angular dark field picture) micrographs of the specimen annealed at 700 °C for 100 h. A dense network of secondary $M_{23}C_6$ carbides has been formed close to the primary $M_{23}C_6$ at the GB. b) Elongated secondary $M_{23}C_6$ carbides are surrounded by γ' precipitates (arrows pointing down) [26]. 13
Figure 9. HAADF micrographs of coarsened primary and secondary $M_{23}C_6$ carbides in specimen annealed at 700 ° C for 1000 h. b) Spherical γ' precipitates surrounding the secondary $M_{23}C_6$ carbides (arrows up) [26]. 14
Figure 10. APT (atom probe tomography) data and concentration profiles across $M_{23}C_6$/γ interfaces after annealing Alloy 617B for 100 hrs. at 700 °C [26] 14
Figure 11. Yield stress as well as average lattice stress *vs.* temperature of the experimental ternary nickel alloys [28]. 16
Figure 12. Predicted lattice stresses (Feltham model) *vs.* observed yield stress values for solution strengthened and precipitation hardened nickel-based alloys 16
Figure 13. Isothermal section of Ni–Cr–Mo ternary phase diagram at 1200 °C [30] 17
Figure 14. Coefficient of thermal expansion of Haynes 242 and 244 compared with other superalloys [35] 22
Figure 15. Yield strength of Haynes 244 compared with Haynes 242 [35] 22
Figure 16. Low cycle fatigue of Haynes 242, 244, and 282 at 760 °C (1400 F) [35] 23
Figure 17. Comparison of stress to produce 1 % creep in 1000 Hours at temperatures of up to 1800 °F (982 °C) (Sheet, Haynesintl.com) [36, 37] 32
Figure 18. High-temperature Vickers Hardness of Haynes 25, 188 and 230 at temperatures of up to 1800 °F (982 °C) (Haynesintl.com) [36, 37] 33
Figure 19. Room-temperature properties of plates of Haynes 230 and 188 compared with Hastelloy X and Inconel 625 after exposure to temperatures of up to 1800 °F (982 °C) (Haynesintl.com) [36, 37] 34
Figure 20. Low cycle fatigue lives at 425 °C of Haynes 188 and 230 compared with Hastelloy X, and Inconel 625 and 617. Left: as-received and right: after 1000 hours at 760°C. (Haynesintl.com) [36, 37] 34
Figure 21. Fabrication of specimens to determine diffusivity and speciation 38

Figure 22. Diffusion specimens for subsequent heat treatment at 550 °C and 650 °C within three consecutive time intervals: 1, 3, and 9 months. 38
Figure 23. PNNL's EasyXAFS 300 for *in-situ* determination of corrosion species by XAFS measurements 39
Figure 24. Inert vacuum furnace attachment to allow for in-situ X-ray absorption spectroscopy (XAS) under in-operando conditions 40
Figure 25. X-ray absorption spectra of corroded foils of chromium (a), nickel (b), and iron (c) compared with the pristine metal foils 41
Figure 26. XAS of Cr-chlorides annealing 1, 2.5, and 5 wt.-% Cr in eutectic NaCl-$MgCl_2$ 42

Tables

Table 1. Alloys considered for compatibility tests in this study 7
Table 2. Nominal alloy composition of Alloy 617 (DIN 2.4663) and Alloy 617B (DIN 2.4673) [22] 11
Table 3. Chemical composition of the nickel-base alloys (wt.-%) [32, 33] 18
Table 4. Brief description of Ni-Cr-Mo alloys Hastelloy N and Haynes 244 20
Table 5. Basic mechanical room temperature properties of Hastelloy N and Haynes 244 21
Table 6. Physio-mechanical properties of alloying metals 24
Table 7. Common nickel-based high temperature alloys and superalloys 25
Table 8. Mechanical room temperature properties of 14 nickel-based alloys and superalloys 29
Table 9. Stress rupture properties of high-temperature alloys between 760-982 °C [36] 32
Table 10. Oxidation resistance after 1000 hours in flowing air between 980 °C and 1150 °C 35
Table 11. Water vapor oxidation (air with 20 % water) of nickel-based alloys after 1008 hours at 982 °C [37] 36

1.0 Introduction and background

Research & development efforts on Molten Salt Reactor (MSR) systems for advancing nuclear reactor technology is focusing on the engineering designs operating with thermal spectra or fast neutron spectra and their deployment is envisioned in the 2030s. In December 2023, the U.S. Nuclear Regulatory Commission (NRC) voted to issue a construction permit to Kairos Power for the Hermes demonstration reactor and its construction has started in July 2024**.** This is the first and only Gen-IV reactor to be approved for construction by the NRC, and the first non-light-water reactor to be permitted in the U.S. in over 50 years [1]. Furthermore, the Abilene Christian University has recently filed an NRC application for the molten salt research reactor (MSRR) construction permit which was approved in September 2004 [2, 3] . The MSRR is a low-power molten salt research reactor in support of academic research. The global MSR research is furthermore impacted by activities in China (e.g., applying an advanced thorium fuel cycle) [4] and Russia (Mosart reactor design) [5, 6]. Halide salt melts are considered as solvent for the fissile/fissionable content and/or as coolant. Fluoride salts have been considered since the early days of MSR technology in the 1960s, and chemical compatibility data of fluoride salt melts with low-chromium nickel-based alloys such as Hastelloy N (standard and modified) and related derivates, are studied since the inception of Molten Salt Reactor Experiment (MSRE) and the Accelerator-driven Transmutation Technology (ADTT) [6-11]. Related research on high-temperature molten-salts as liquid fuel and/or as primary coolant focused on fluoride salts because of their relatively noncorrosive behavior, neutron moderation, and the chemical stability at temperatures of 700 °C. Chloride salts on the other hand, are an alternative option and are considered by the latest commercial designs e.g. of Exodys Energy MCSFR, TerraPower MCFR, Moltex SSR-W300 [12-14], but their *in-operando* behavior is less well understood and additional data are needed for technological deployment and licensing. Chloride salt melts are lesser moderators and allow for a faster (harder) neutron spectrum. The deployment of a harder neutron spectrum allows spent nuclear fuel as potential fissile fuel source and therefore low long-term operational costs. Chloride melts are sufficient solvents for actinides and lanthanides, but, because of the low electrochemical potentials of metal chlorides compared with metal fluorides, chloride salt systems in general show enhanced corrosion rates compared with fluoride salt systems. Chloride-based salts have been used in the fuel-reprocessing scheme developed for the integral fast reactor [15].

Experiments on corrosion effects with molten salts date back to the Aircraft Reactor Experiment as early as 1940 [7] and research on chemical compatibility of steel and nickel-based alloys with fluoride and chloride salts will continue for many years to come. Corrosion processes of alloys in chloride salt melts are probably more complex than those in fluoride salt melts. Consequently, the knowledge base for structural materials tolerant to chloride-based salt melts is not as mature as the one for fluoride-based salts [15]. A confident structural material selection has yet to be provided for any chloride salt-based molten salt reactors and an ASME-coded alloy for MSR deployment is unavailable for years to come.

Corrosion of stainless steel (typically >11 wt. % Cr) or low-chromium nickel-based alloys is typically initiated by the solubility of Cr as $CrCl_2$ or as $CrCl_3$ species in molten chloride salt melts, purely as consequence of thermodynamics and independent of the selected structural material as containment. In contact with molten chloride salt melt, chromium does not form protective Cr_2O_3 or Cr_3O_4 chromite layers nor protective $FeCr_2O_4$ magnetite or spinel-type layers. Because of the low electrochemical potentials of chromium chlorides, chromium is unstable (active) and dissolves as $CrCl_2$ and $CrCl_3$ chloride species and become part of the molten salt phase. Additionally, the formation of corundum (Al_2O_3) or $MgAl_2O_4$ by alloying with aluminum is not

likely to be a valid option based on thermodynamics. Compact oxide layers are often used as corrosion barriers in the nuclear reactor systems. For example, in the liquid lead-bismuth cooled reactor, the oxide layers formed on the structure material are effective barriers to mitigate the corrosion by the liquid metal coolant. In molten halide salt melts, the formation of an oxide barrier layer is thermodynamically infeasible because of the presence of chlorine or fluorine ions and the resulting formation of stable metal halides. Selective alloying metal corrosion in molten halide salts therefore proceeds via active dissolution and without the presence of oxide layer or a mechanism of “fluxing” which is a synergistic process of degrading the metal by alternate chloride dissolution and oxide scale formation.

1.1 Thermodynamic considerations

Corrosion of structural materials in molten salts is largely an irreversible electrochemical process involving the anodic dissolution of metal and the cathodic evolution of the oxidant in the salt. The anodic dissolution of metal can be expressed as:

$$M \rightarrow M^{n+} + ne^{-} \tag{1}$$

where *M* represents the metallic element such as Ni, Fe, Cr, Co in the structural material, *n* is the number of exchanged electrons.
The cathodic reduction of oxidant in the salt can be written as:

$$Ox + ne^{-} \rightarrow Red \tag{2}$$

where *Ox* and *Red* represent the oxidant and its corresponding reductant, respectively.
The combination of the partial anodic reaction (1) and the partial cathodic reaction (2) yields the overall electrochemical corrosion reaction:

$$M + Ox \rightarrow M^{n+} + Red \tag{3}$$

To allow the corrosion reaction to occur spontaneously, the change of the Gibbs free energy of the corrosion reaction must be negative. For an electrochemical reaction, the Gibbs free energy change can be expressed as:

$$\Delta G = -nF\Delta E \tag{4}$$

where ΔG is the Gibbs free energy change per mole of reaction, J/mol; F is Faraday constant, 96,485 C/mol; $\Delta E = E_c - E_a$ is the potential difference while E_a and E_c are the redox potential of the anodic electrode reaction and cathodic electrode reaction in V, respectively.
If E_c is more positive (noble) than E_a, i.e., $\Delta G < 0$, the metal in molten salt will be spontaneously corroded. The redox potential for the half-cell electrode reaction relates to the activity of the corresponding species according to the Nernst equation:

$$E_a = E_a^0 + \frac{RT}{nF} ln \frac{a_M^{n+}}{a_M} \tag{5}$$

$$E_c = E_C^0 + \frac{RT}{nF} ln \frac{a_{Ox}}{a_{Red}} \tag{6}$$

where E_a^0 and E_c^0 are the corresponding standard electrode potentials and *R* is the gas constant, 8.314 J/K/mol, while a_{Mn+}, a_{Ox} and a_{Red} are the activities for the relevant species. For pure metals a_M is set to 1.
The standard electrode potential E^0 can be calculated through the Gibbs free energy of its reactants and products. To calculate the E^0 of M^{n+}/M versus the standard Cl_2/Cl^- reference, the following two half-cell reactions are considered:

$$M + nCl^- \leftrightarrow MCl_n + ne^- \tag{7}$$

$$\frac{n}{2}Cl_2 + ne^- \leftrightarrow nCl^- \tag{8}$$

Combining the half-cell reactions yields to:

$$M + \frac{n}{2}Cl_2 \leftrightarrow MCl_n \tag{9}$$

The change in Gibbs free energy per mole for (9) equals the standard Gibbs free energy of the formation of MCl_n and therefore:

$$\Delta G = \Delta G_f^0\ (MCl_n) \tag{10}$$

Considering the standard electrode potential M^{n+}/M, the electrode reaction can be calculated as following:

$$E^0_{Mn+/M}\left(vs.\frac{Cl_2}{Cl^-}\right) = \frac{\Delta G_f^0(MCl_n)}{nF} \tag{11}$$

The value of $\Delta G_f^0\ (MCl_n)$ is changing as a function of temperature and can be extracted from thermochemical properties tables. In many cases, melting temperature of pure MCl_n is higher than that of the molten salt mixture in which the MCl_n is present as liquid. To calculate the Gibbs free energy of these chlorides, the supercooled state should be used which is a summation of ΔG_f^0 at solid state and the Gibbs energy of fusion. The latter can be calculated by the values of enthalpy, entropy, and heat capacity at liquid and solid state [16].
Once the standard electrode potential for the redox couple is known and considering the Nernst equation, the redox potential at given activities and temperatures can be calculated. The calculated redox potentials of active-passive redox pairs M^{n+}/M, representing alloying metals in molten chloride salt are displayed in Figure 1.

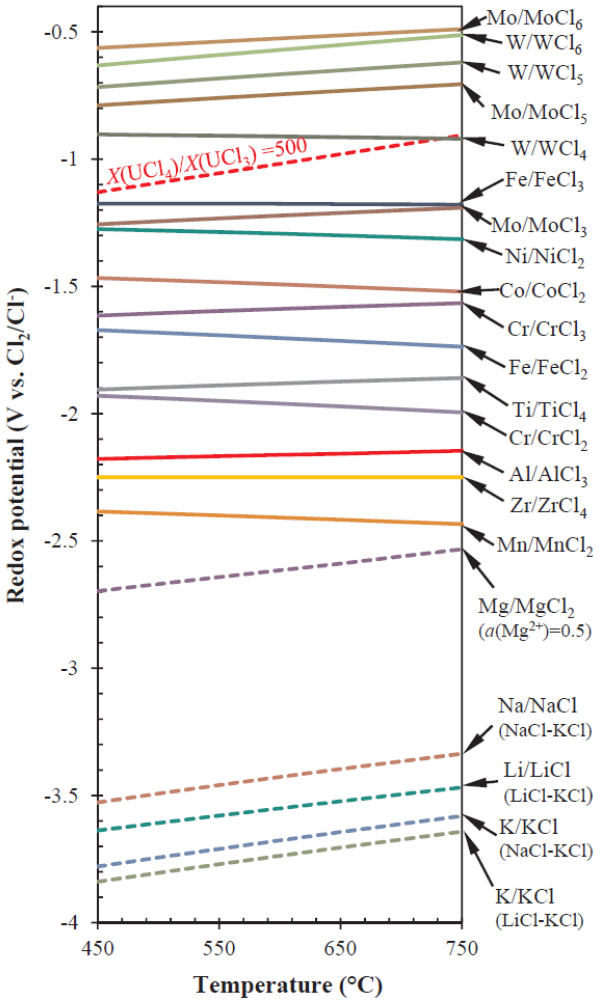

Figure 1. Redox potentials of various redox couples as a function of temperature in chloride salts. *Solid line*: metal dissolution at a_{Mn^+} of 1 μM/L. *Dotted line*: reduction of oxidants [16].

At the solid line in Figure 1, the metal *M* equilibrates with M^{n+} with an activity of 10^{-6} M/L in the melt. At potentials below the solid line, the metal is expected to be thermodynamically stable. However, if an oxidant with its reduction potential above the solid line is present in the melt, and therefore:

$$E_{Ox/Red} > E_{Mn+/M} \quad (12)$$

At this, the metal will be corroded until the concentration of dissolved M^{n+} elevates to the equilibrium level defines as:

$$E_{Ox/Red} = E_{Mn+/M} \quad (13)$$

1.2 NaCl-$MgCl_2$ salt system

The phase constitution of the NaCl-$MgCl_2$ system has been carefully measured in the past by thermal analysis, differential thermal analysis, and x-ray diffraction [17]. The reported binary and ternary phases are NaCl, $MgCl_2$, $NaMgCl_3$, Na_2MgCl_4, and $NaMg_2Cl_5$. The existence of the ternary compound $NaMg_2Cl_5$ is uncertain. No border solid solubility is reported, and the limiting slopes of the NaCl and $MgCl_2$ liquidus curves are described by the following equation [17] where ΔH^0_{fusion} and T_{fusion} are the enthalpy and temperature of melting of the pure salt, respectively.

$$\lim X_m \to 1 \left(\frac{dX_m^{liquidus}}{dT}\right) = \frac{\Delta H^0_{fusion}}{RT^2_{fusion}} \quad (14)$$

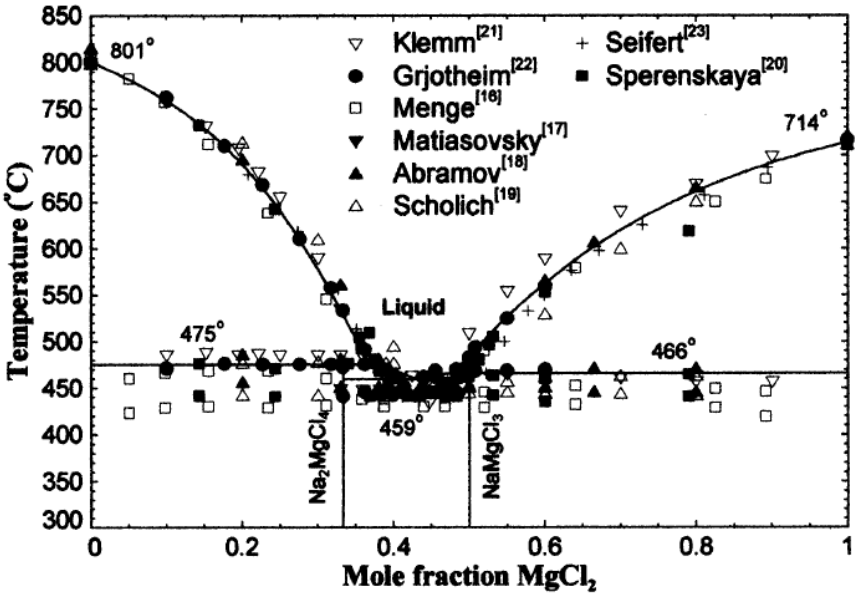

Figure 2. The NaCl-$MgCl_2$ system: Calculated and experimental data [17]

The eutectic temperature in the pseudo-binary NaCl-$MgCl_2$ system is 459 °C (732 K) while the peritectic temperatures for either peritectic reaction are 475 °C for $L + NaCl \rightarrow Na_2MgCl_4$ and 466 °C for $L + MgCl_2 \rightarrow NaMgCl_3$, respectively (Figure 2).

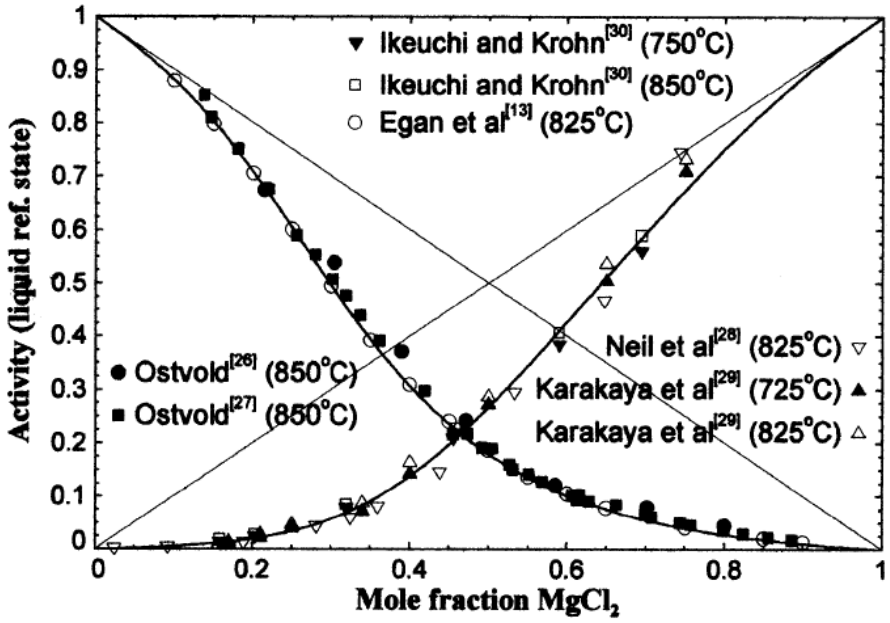

Figure 3. NaCl-$MgCl_2$ system: Calculated activities in the liquid at 800 °C [17]

The pseudo-binary system NaCl-$MgCl_2$ shows a strong negative deviation from ideal mixing with activity coefficients noticeably smaller than unity (Figure 3).

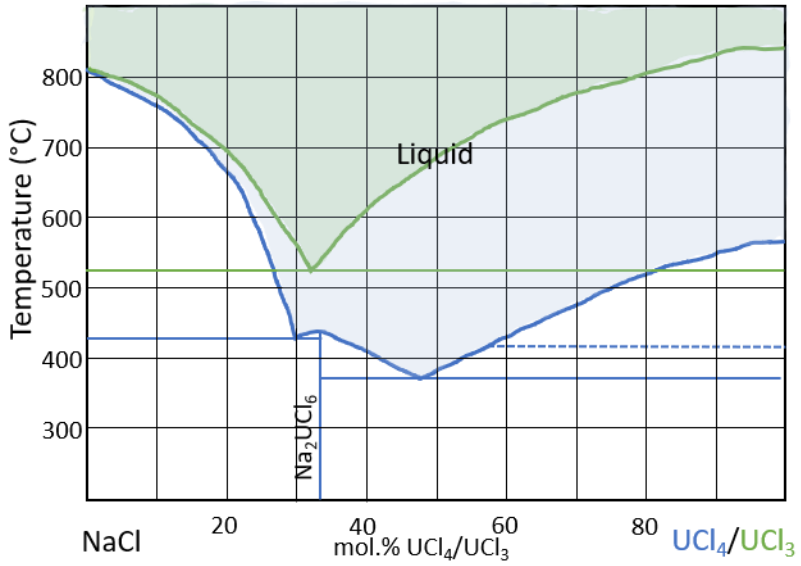

Figure 4. The Systems NaCl-UCl_3 and NaCl-UCl_4 [18]

The system NaCl-$MgCl_2$, because of the ternary phases Na_2MgCl_4 and $NaMgCl_3$, shows a wide solubility range of the *liquid* phase with a low eutectic temperature similar to the fuel system NaCl-UF_4 (Figure 4). Therefore, it is fair to consider the binary NaCl-$MgCl_2$ as a suitable surrogate system for corrosion experiments with stainless steel and nickel-based alloys, assuming the viscosities and chemical activities are somewhat similar as well.

1.3 Alloy systems

In this study we will test the compatibility of SS316, Inconel 625, and Inconel 617 with eutectic Na-Mg-Cl salt melts at 550°C and 650°C (Table 1).

Table 1. Alloys considered for compatibility tests in this study

SS316 **UNS S31600**	**Fe bal. <0.03% C 16-18.5% Cr 10-14% Ni 2-3% Mo <2% Mn <1% Si <0.045% P <0.03% S** Grade 316 is the standard molybdenum-bearing grade, second in importance to 304 amongst the austenitic stainless steels. The molybdenum content gives 316 better overall corrosion resistant properties than Grade 304, particularly higher resistance to pitting and crevice corrosion in chloride environments. It has excellent forming and welding characteristics. It is readily brake or roll formed into a variety of parts for applications in the industrial, architectural, and transportation fields. Post-weld annealing is not required when welding thin sections. This alloy is ASME coded for nuclear applications.
Inconel 617 **UNS N06617**	**Ni 44.5 min. Cr 20-24 Co 10-15 Mo 8-10 Al 0.8-1.5 Fe 3 max. Si 1 max. Ti 0.6 max.** Inconel 617 is a solid-solution strengthened, nickel-chromium-cobalt-molybdenum alloy with an exceptional combination of high-temperature strength and oxidation resistance. This alloy also has excellent resistance to a wide range of corrosive environments, and it is readily formed and welded by conventional techniques. This alloy combines high strength and oxidation resistance at temperatures over 980 °C. Alloy 617 is used for components such as ducting, combustion cans, and transition liners in both aircraft and land-based gas turbines. Because of its resistance to high-temperature corrosion, it is used for catalyst-grid supports in the production of nitric acid, for heat-treating baskets, and for reduction boats in the refining of molybdenum. This alloy is ASME coded for nuclear applications.
Inconel 625 **UNS N06625**	**Ni 58 min. Cr 20-23 Mo 8-10 Nb 3.15-4.15 Fe 5 max.** Inconel 625 is characterized by high tensile strength, high rupture strength, excellent heat resistance, great oxidation resistance, and excellent weldability. Alloy 625 offers a wide range of desirable properties such as high temperature corrosion resistance and high temperature strength. The niobium content combined with molybdenum distorts the alloy's atomic matrix, imparting particularly high strength in annealed conditions without a specific strengthening heat treatment. The high quantities of nickel and chromium together give the material its exceptional corrosion resistance. Inconel alloy 625 is an approved material of construction under the Boiler and Pressure Vessel Code of the American Society of Mechanical Engineers (ASME) but not ASME coded for nuclear deployment.

1.4 Iron-chromium-nickel-based systems

In this section, the underlying principles of high-temperature alloys (superalloys) are evaluated and discussed in terms of general materials science and fundamental metallurgy.

Nickel and, more recently, cobalt-based superalloys have dominated the scene of high-temperature structural materials because of some of their basic attributes. Both consist of matrix phases that have close-packed structures (fcc or hcp, respectively), which are associated with inherent ductility at ambient temperatures and a low diffusivity due to their close packing, resulting in good creep resistance [19]. High strength and good creep resistance at elevated temperatures arise due to stronger bonding, which is reflected by a high elastic modulus. Superalloys contain one or more dispersed ordered intermetallic phases to varying extents. Generally, the wrought variety has a smaller volume fraction of intermetallic phases than the cast variety. The fundamental point of the design of these alloys is to ensure that the matrix solid solution phase and the dispersed intermetallic phases are coherent with each other and, therefore, resistant to coarsening of the dispersed phase at high operating temperatures.

Alloy strengthening is achieved by solid solution (solid solution strengthening) and hard particle dispersion (precipitation hardening) and the microstructural stability at elevated operating temperature arises due to the very close matching of the lattices of the matrix and precipitate phases.

The use of refractory elements as alloying metals gives rise to solid solution strengthening of the matrix and stable second-phase dispersion for arresting the grain growth. These additions have yielded some materials for use at temperatures exceeding 1000 °C [19]. The high creep rate at elevated temperatures and high ductile-to-brittle transition temperature associated with the bcc structure along with poor oxidation resistance remain as the main obstacles for their extensive applications.

Various alloying additions have been carried out to improve the properties of steel under extreme conditions. Among them, the addition of Ni and Cr have been most rewarding alloying additions. Corrosion properties of steel significantly improve by the addition of Cr and Ni and detailed mapping of the alloy system has been developed after 1920 [20]. An isothermal section of the ternary Fe-Ni-Cr system is provided in Figure 5 [19]. Different phase fields marked in the phase diagram are used to highlight various commercial alloys developed using this ternary phase diagram as the basic entity. Major commercial alloys developed using these elements as their base are superalloys and stainless steels. Nickel-chrome alloys have been used for various high-temperature applications but with the demand of higher operating temperatures in high-tech areas, the development of more complex alloys is required.

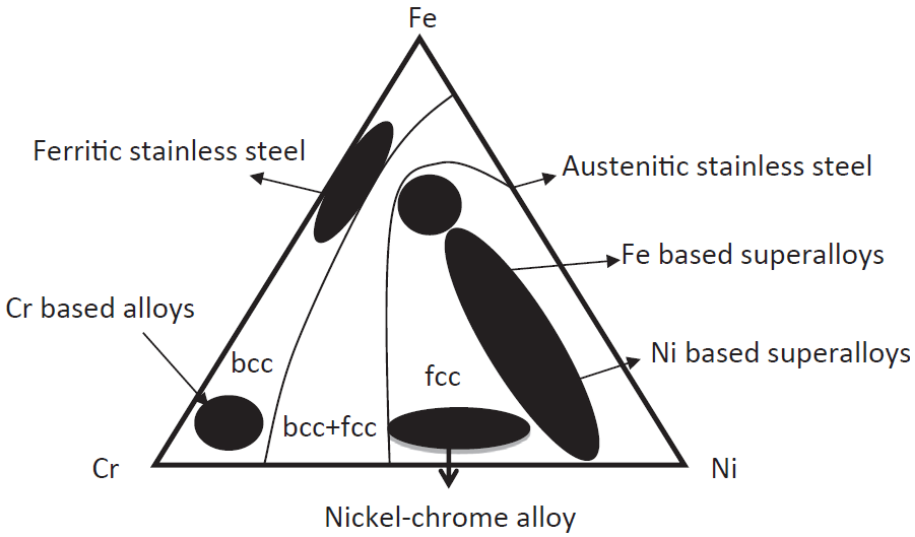

Figure 5. Schematic representation of the isothermal section of the ternary Fe-Cr-Ni-based system [19].

With the demands of Gen-IV reactor technology, alloys must provide adequate high-temperature properties such as corrosion resistance, mechanical yield strength and creep resistance at temperatures beyond 600 °C. This absolutely requires limiting the content on iron and manganese to <5 wt.-% and <3 wt.%, respectively. Also, the content in silicon should be reduced to <1wt.%. The content in critical and less abundant refractory metals, on the other hand, will have to be increased to double-digit wt.% numbers in order to meet the design requirement of the deployed technology. At this, cobalt contents of 10-15 wt.%, molybdenum concentrations of up to 10 wt.%, and tungsten concentration of up to 15 wt.% might be necessary and unavoidable to successfully and safely operate high-temperature engineering designs for four to six decades.

1.5 Development of high-temperature alloys for nuclear applications

Components of nuclear reactor systems are designed in accordance with applicable provisions of the ASME Boiler and Pressure Vessel Code. For Class 1 structural components at relatively low temperatures of 371 °C (700 °F) or below, ferritic steels, and for 427 °C (800 °F) or below, austenitic steels and high-nickel alloys are listed. For components at higher temperatures, code case N-47 is applicable and alloys are permitted for deployment at elevated temperatures for service life of up to 300,000 hours (34 years) [21]. Until recently, there were only five alloys allowed for use in high temperature nuclear components: ferritic 2.25Cr- 1Mo and V-modified 9Cr-1Mo steels, austenitic Types 304 and 316 stainless steels, and the high nickel austenitic Alloy 800H. The chromium-cobalt-molybdenum Alloy 617 was added to the ASME Boiler and Pressure Vessel code in 2019 and is the first high-temperature material cleared for commercial use since the 1990s. Alloy 617 can be deployed at temperatures of 954 °C (1750°F) for 100,000 hours (11 years).

The history of Alloy 617 dates to the 1970s when Eiselstein at al. developed Alloy 617 and applied for a patent (U.S. Patent 3,859,060). This nickel-chromium-cobalt-molybdenum alloy was characterized by good strength at temperatures up to 2000 °F combined with excellent resistance to cyclic oxidation, and structural stability as well as excellent workability [22]. Alloy

617 was specifically designed for high-temperature applications up to 1200 °C. It derives its high creep strength through both: solid solution hardening and carbide precipitation. Since then, Alloy 617 has been broadly used in industrial gas turbines and components in petrochemical plants at typical operating temperatures of 800 °C and above. In the 1980s, Alloy 617 was selected as a suitable alloy for the European high-temperature reactor (HTR) project within the Prototype Nuclear Process Heat program [23]. Alloy 617 has been thoroughly investigated and the general result of this investigation was that Alloy 617 is suitable for use in high-temperature reactors.

Alloy 617 (UNS N06617) was selected as a candidate material for the first boilers in the European USC 700 °C boiler projects due to its combination of high creep resistance, good workability, and weldability. Alloy 617 was also approved for pressure vessel application by VdTÜV and finally the ASME Boiler and Pressure Vessel code. However, when designing the first USC boilers (700 °C boilers) in Europe, it became clear that the maximum allowed 100,000 h creep rupture strength of 95 MPa was not sufficient. To further increase its creep strength and, at the same time, increase the ductility in the temperature range 650–750 °C, a modified version of Alloy 617 with strict tolerances on alloying elements and additions of boron was designed. This boron-modified alloy is labeled Alloy 617B containing additional 0.001 - 0.005 wt.% boron.

1.6 Metallurgy of Alloy 617

In this section the properties and metallurgy of Alloy 617 are discussed since it represents a textbook example of how a suitable high-temperature alloy can be designed and further optimized for deployment in an engineering design under extreme conditions.

1.6.1 Solution strengthening and precipitation hardening of Alloy 617

Alloy 617 is an austenitic nickel alloy containing approximately 55 wt.% nickel. Similar to most nickel-based high-temperature alloys, the desired properties such as creep strength and related high-temperature physio-mechanical properties are derived basically from three mechanisms:

- Solid solution strengthening
- Carbide formation, $M_{23}C_6$, but also M_6C and Ti(C,N)
- Formation of ordered intermetallic phases such as the γ'-phase $Ni_3(Al,Ti)$.

The alloying elements Cr, Co, and Mo are added to strengthen the nickel-based solid solution, and aluminum and titanium are added to form γ'-precipitates. While solid solution strengthening and carbide strengthening are predominant at high temperatures, γ'- formation is an important strengthening factor at intermediate temperatures (Figure 6).

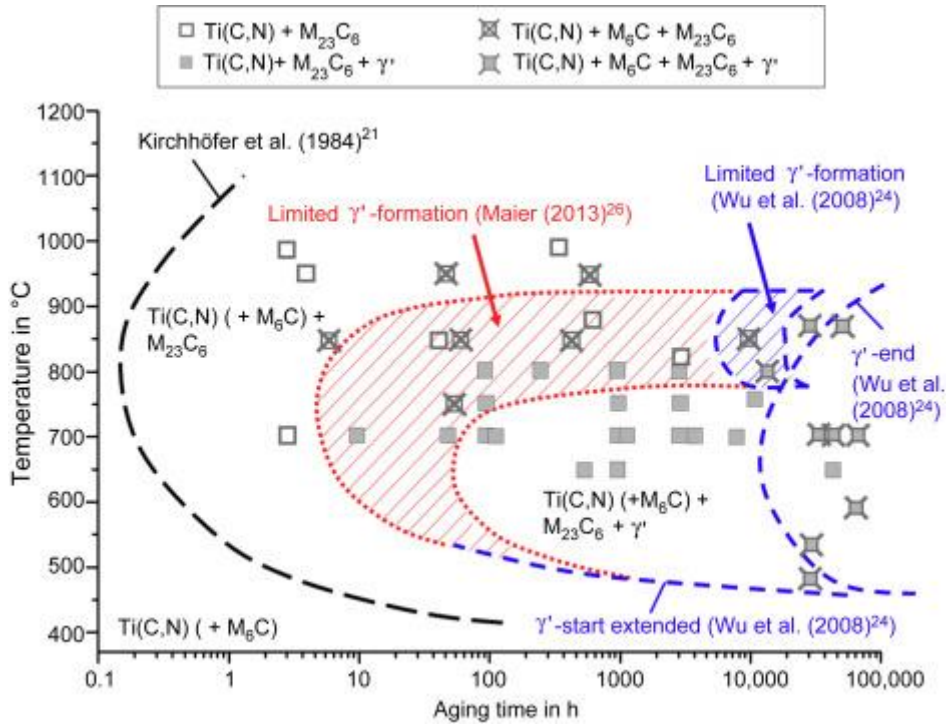

Figure 6. Time-temperature-transformation diagram of boron-modified Alloy 617B (Alloy 617mod) [24]

The time-temperature-transformations diagram of Alloy 617B shows that γ'-based precipitation hardening is mostly observed in an intermediate temperature range, between 500 and 900 °C, and γ' is redissolved at high temperatures of 1000 °C or above. Compared to standard Alloy 617, Alloy 617B it is characterized by a narrower concentration range of alloying elements. The lower limits of the solid solution–strengthening elements chromium and cobalt were increased, as well as the inventory on precipitation-strengthening elements aluminum and titanium. Furthermore, the allowable amount of potentially detrimental softening elements such as Fe, Si, and Mn was decreased.

Table 2. Nominal alloy composition of Alloy 617 (DIN 2.4663) and Alloy 617B (DIN 2.4673) [22]

	Alloy 617 ASME SB 168	**Alloy 617 VdTÜV data sheet 485**	**Alloy 617B VdTÜV data sheet 573**
UNS	N06617	–	N06617
DIN-No	–	2.4663	2.4673
Ni	≥44.5	Balance	Balance
Cr	20.0–24.0	20.0–23.0	21–23
Co	10.0–15.0	10.0–13.0	11–13
Mo	8.0–10.0	8.0–10.0	8–10
Ti	≤0.6	0.20–0.50	0.25–0.5
Al	0.8–1.5	0.60–1.50	0.8–1.3
B	≤0.006	–	0.001–0.005
Fe	≤3	≤2.00	≤1.5
Mn	≤1.0	≤0.70	<0.5

Si	≤1.0	≤0.70	<0.3
C	0.05–0.15	0.050–0.100	0.05–0.08
P	–	≤0.012	<0.012
Cu	≤0.5		–
S	≤0.015	≤0.008	<0.008
V	–	–	≤0.6
Nb	–	–	≤0.6
As	–	≤0.010	–
Bi	–	≤0.010	–

1.6.2 Creep strength of Alloy 617and narrowing chemical bandwidth

The major benefit of controlling the alloying inventory within a narrower bandwidth lies in the reduced margin of error of the measured creep strength data. Creep rupture data can indeed exhibit considerable scattering as shown in Figure 7.

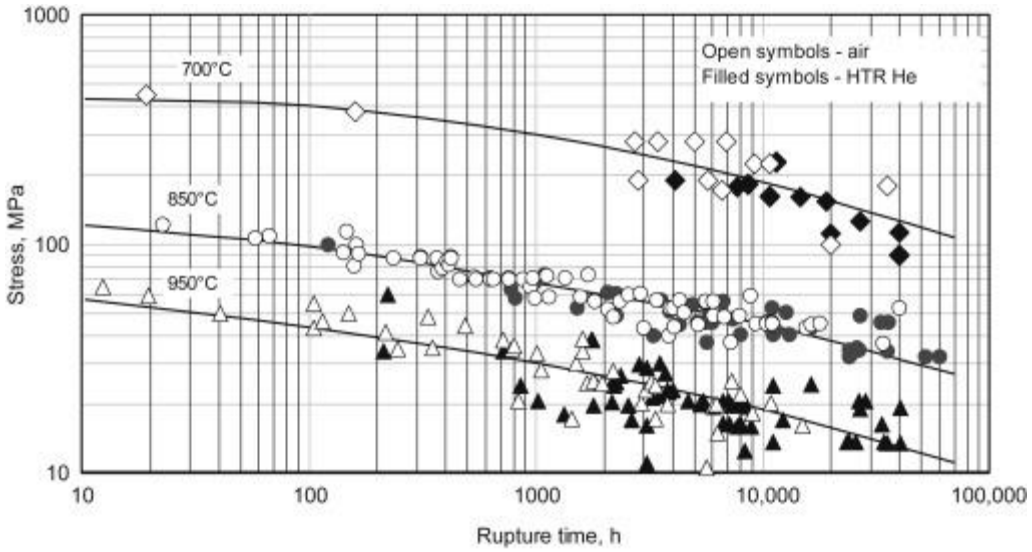

Figure 7. Creep rupture strength of Alloy 617 as a function of rupture time [22]

The broad scatter of creep rupture data impacts the quality of performance assessment and enhances the probability of design failure by underperforming alloy compositions. The broad scatter as shown in Figure 7 is not only caused by alloy composition at the low end of bandwidth for the concentrations of Cr, Co, and Mo, but also derived by differences in heat treatment, grains sizes, and the particle distribution. As the data show, narrowing the scatter of alloy composition by increasing the lower limits of the strengthening alloying metals, the creep rupture data will be shifted to the upper limit of the scatter band, ensuring adequate performance with lower uncertainties in performance evaluation.

1.6.2.1 Heat treatment of Alloy 617

Solution annealing of Alloy 617 may be carried over a temperature range from 1140–1200 °C. However, high solution-annealing temperatures above 1180 °C should be avoided to reduce the risk of grain coarsening. Additional stress relief annealing at 980 °C for 3 h is recommended, especially for large, welded components fabricated from Alloy 617. Like most high-strength

alloys, Alloy 617 is susceptible to stress relaxation cracking in the temperature window between 650 and 750 °C. This phenomenon has been largely investigated on Alloy 800H (UNS N08810) [25]. While the mechanism is still not clear, it has been demonstrated for many alloys, that stress relief annealing also called relaxation annealing prevents this type of stress corrosion cracking [25].

Alloy 617 shows grain sizes typically between 100 and 200 µm. Smaller grains do favor higher fatigue resistance but result in lower creep resistance. Stress relief annealing at 980 °C induces the formation of secondary carbide precipitates of the type $Cr_{23}C_6$ along grain boundaries and within the grains [24]. To a much lesser degree, primary molybdenum rich M_6C carbides may also be present. Solution annealing followed by stress relief annealing is not sufficient to induce the formation of γ'-precipitates. However, these precipitates will form if annealing within an intermediate temperature window (500-900 °C) continues for at least 10 hours as TEM investigations have shown [24].

1.6.3 Microstructure of Alloy 617 and Alloy 617B

Annealing at 700 °C for 100 h produced a dense network of secondary carbides close to the grain-boundary (GB) region, and γ' particles nucleated at the face sites of secondary $M_{23}C_6$ carbides (Figure 8). The γ' particles undergo coarsening during prolonged annealing and are ellipsoidal in shape (Figure 9) [26].

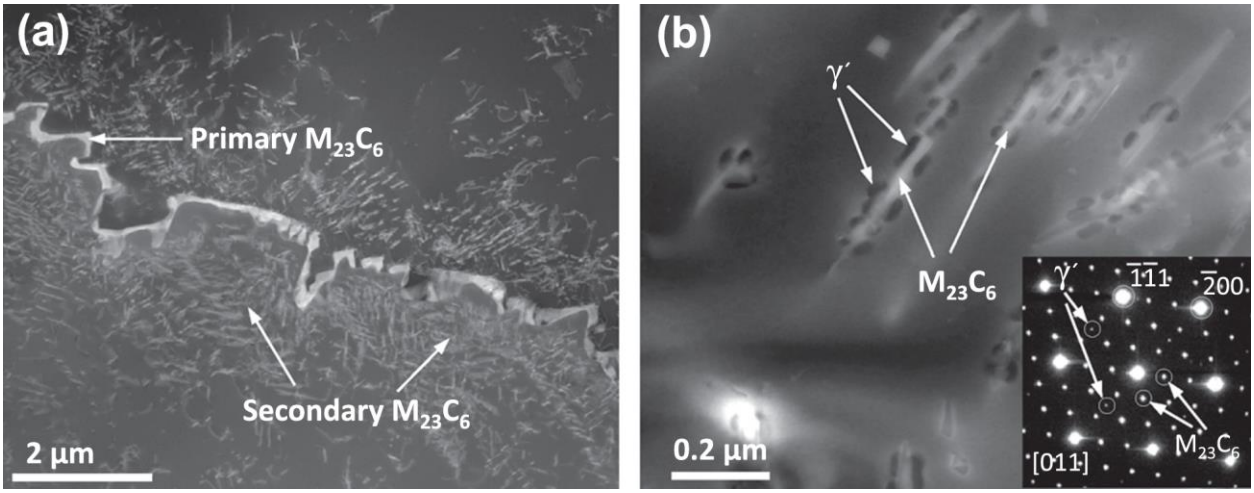

Figure 8. a) HAADF (high-angle angular dark field picture) micrographs of the specimen annealed at 700 °C for 100 h. A dense network of secondary $M_{23}C_6$ carbides has been formed close to the primary $M_{23}C_6$ at the GB. b) Elongated secondary $M_{23}C_6$ carbides are surrounded by γ' precipitates (arrows pointing down) [26].

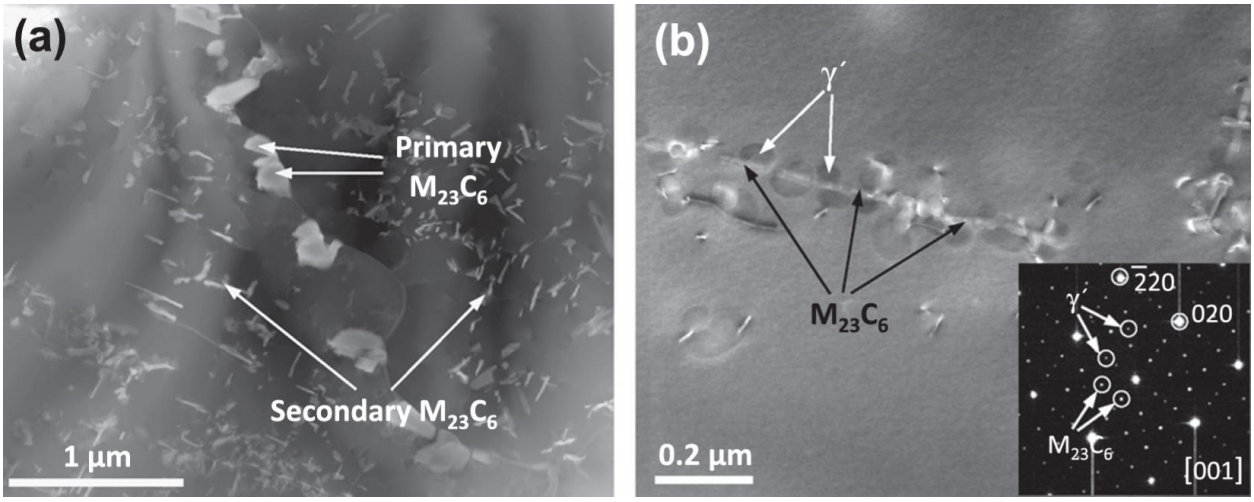

Figure 9. HAADF micrographs of coarsened primary and secondary $M_{23}C_6$ carbides in specimen annealed at 700 ° C for 1000 h. b) Spherical γ' precipitates surrounding the secondary $M_{23}C_6$ carbides (arrows up) [26].

Annealing of Alloy 617 for long durations (one-year) at 700 °C, increases its yield strength and tensile strength considerably, while ductility is not impacted significantly. This strengthening effect is explained by the formation of small γ' precipitates, a mechanism known from other precipitation strengthened nickel-based superalloys. The overall precipitation strengthening is achieved by the formation of $M_{23}C_6$ carbides along the grain boundary (primary) and within the grain (secondary) alongside with γ' $Ni_3(Al,Ti)$ precipitates with an average size of 50 nm.

Furthermore, boron with concentrations of 10-50 ppm has a significant effect on the strength and the ductility of Alloy 617. The mechanism of the boron segregation is not well understood. However, it is known from other nickel-based superalloys such as Alloy 716 that boron tends to segregate at grain boundaries [27]. Recent atom probe analysis in boron-modified Alloy 617B show that boron segregates at the grain boundaries as well as at the matrix/carbide interfaces (Figure 10) [26].

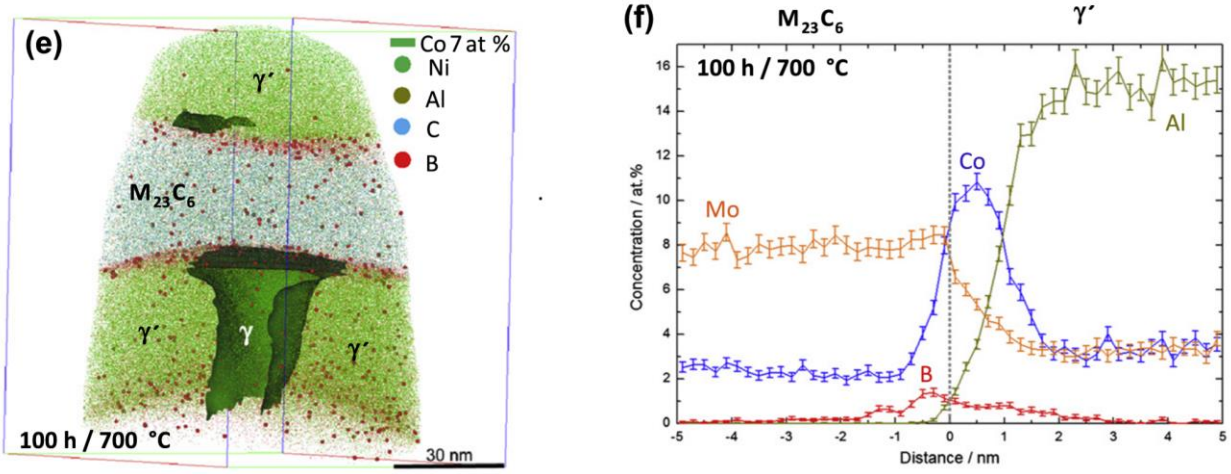

Figure 10. APT (atom probe tomography) data and concentration profiles across $M_{23}C_6$/γ interfaces after annealing Alloy 617B for 100 hrs. at 700 °C [26].

In heat-treated Alloy 617B (100 hrs @ 700 °C) boron enriches at the $M_{23}C_6/\gamma$ phase boundary. TEM and APT observations show that γ'precipitates are adjacent to $M_{23}C_6$ particles as shown in Figure 9. Enrichments of boron at the $M_{23}C_6/\gamma$' interfaces are significant and might explain the enhancement in physio-mechanical properties of Alloy 617B compared with standard Alloy 617. A 0.5-2 at.% boron increase within a 3-4 nm width was measured at the interface region. In addition to the boron enrichment at the $M_{23}C_6/\gamma$' interface, cobalt concentrations are increased as well [26]. The γ' phase showed an increase of 8-9 at.% cobalt within a width of 2-3 nm.

1.6.4 Solid Solution strengthening of high temperature alloys

In this section, the importance of solute solution strengthening (hardening) of high temperature alloys is examined. The development of new nickel superalloys is as time consuming as it is expensive. Having the ability to select promising alloy compositions for further testing would streamline the overall process and avoid unnecessary experimental testing. If we could, as a first step, predict the yield stress of a nickel-rich solid solution, the yield strength could be then, in conjunction with models describing the strengthening effect of precipitates, predict the yield strength of the multiphase alloy. In this context, the Feltham model was applied by Roth et al. in 1997 to experimental and commercial data and was found to predict the yield stress well for alloys that were solely solid solution strengthened [28].

The trough model visualizes a situation in which dislocations reside in *troughs* which are stable low energy positions for the line dislocation. Troughs also exist within pure materials but are enhanced by the presence of solute atoms. To propagate slip, the dislocation must break out of the trough. This is thought to occur by the nucleation of a bulge from the trough, and then the rest of the dislocation breaks free by a rapid *unzipping* process [28].

The yield strength of a Ni-based solid solution was predicted based on the lattice stress using the Feltham model (Figure 11) and the following relation was obtained:

$$T\left(\frac{\tau}{\mu}\right)^{1/2} = K_1 - K_2\tau \tag{15}$$

For absolute temperature T, shear stress τ, shear modulus μ and the constants k_1 and k_2 which are constant for an alloy, but are both functions of the alloy's solute concentration [28]. The value of K_2 was determined by fitting the measured K_1 values to the predicted yield stresses for the different experimental alloys. The average value for K_2 was set to 0.22 K MPa^{-1}, and therefore:

$$T\left(\frac{\tau}{\mu}\right)^{1/2} = K_1 - 0.22\tau \tag{16}$$

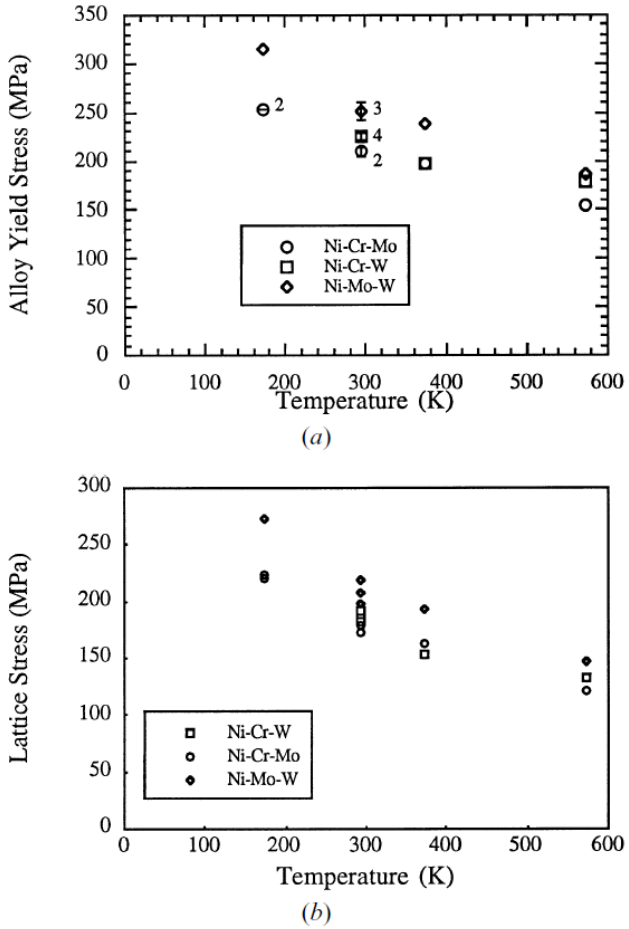

Figure 11. Yield stress as well as average lattice stress *vs.* temperature of the experimental ternary nickel alloys [28].

The comparison between the predicted lattice stresses and actual yield stress values by applying the Feltham model are shown in Figure 12. As one would expect, precipitation hardened nickel-based alloys such as Inconel 625 and Haynes 230 show lower predicted yield stresses than the experimental values indicate.

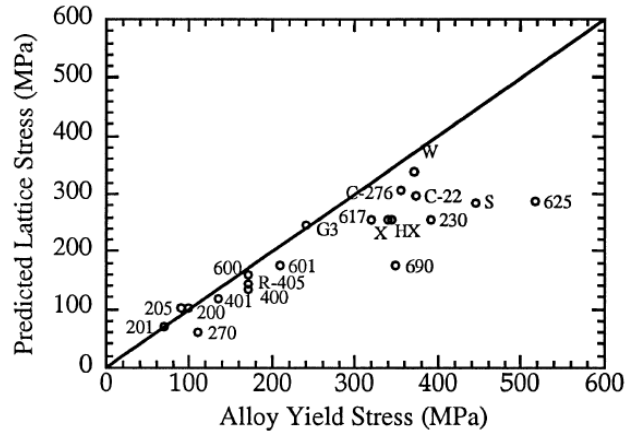

Figure 12. Predicted lattice stresses (Feltham model) *vs.* observed yield stress values for solution strengthened and precipitation hardened nickel-based alloys

In addition, precipitation-hardened alloys such as Inconel 617, 625, 690, Haynes 230, Hastelloy C-22, C-276 also show lower predicted lattice stresses compared with experimental data [28] and computational efforts at the current state might not be sufficient to determine physio-mechanical properties of complex superalloys.

In general, nickel-chromium-molybdenum (-tungsten) superalloys such as the Hastelloys C-4, C-22, C-276, Hastelloy S, Haynes 242, Haynes 244, Alloy 625, and Alloy 686 are used for applications requiring very high corrosion and oxidation resistance. Some of these alloys are candidate materials for long-term high-temperature applications because of their sufficient mechanical strength and oxidation resistance, as well as superior form stability (creep resistance) between 700 °C and 950 °C. These materials are mostly deployed as solid solution strengthened alloys and are generally considered not hardenable by conventional ageing treatments. Prolonged ageing in the temperature range of 400 °C to 700 °C will, however, result in the precipitation of a long range ordered low-enthalpy $Ni_2(Cr,Mo,W)$ phase, with orthorhombic Pt_2Mo prototype crystal structure [29] from the disordered fcc matrix within these alloys. The precipitation of $Ni_2(Cr,Mo,W)$ will therefore initiate age-hardening and its total yield will change with Cr to Mo and Cr to W ratio. The Pt_2Mo-type phase shows a solvus withing the γ-solid solution phase at temperatures below about 620 °C [29]. The solvus temperature, however, increases towards higher Mo/Cr ratios, from 628 °C (Mo/Cr = 0) to 773 °C (ratio Mo/C = 1) along the dotted line in Figure 13 from point 1 to point 8 [30]. Therefore, with increasing Mo/Cr ratios Ni-Cr-Mo-W alloys will likely see an increased hardening effect by Pt_2Mo-type phase precipitation, which is more pronounced with increased molybdenum concentration and the extent of the $Ni_2(Cr,Mo,W)$ phase field.

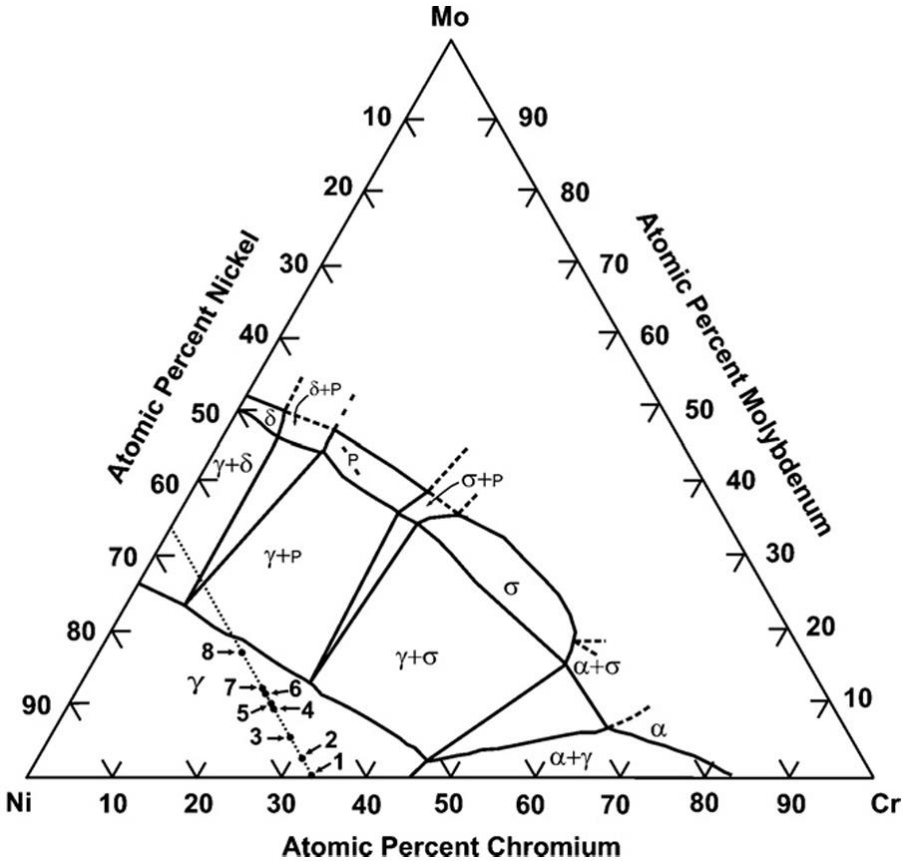

Figure 13. Isothermal section of Ni–Cr–Mo ternary phase diagram at 1200 °C [30]

1.7 Suitable alloys for MSR application

In this section, suitable alloys for MSR-type applications are evaluated. It must be specified, that most stainless-steel alloys, such as SS31600, or nickel-based alloys like Inconel 617 and Inconel 625 are not well suited for MSR deployment since they are lacking chemical compatibility due to their high chromium content. As discussed previously, (Chapter 1.0) the alloying metal chromium is the most active alloying metal in contact with molten salt melts and the subsequent formation of soluble chromium halides will induce intense dealloying, void-formation, and strongly reduced grain boundary strength. Data on standard free energies of formation for species in fuel salts [31] reveal that chromium is much more readily attacked than iron, nickel, or molybdenum. Ni-base alloys, more specifically Hastelloy N and its later modifications, have been considered to be more promising for their use in molten salts and have received significant attention during the MSRE research at ORNL [31]. The chemistry of Hastelloy N was specifically tailored to achieve compatibility with fuel salts containing UF_4 by simply allowing the melt to equilibrate with the alloy. The necessity of low-chromium concentration in MSR containment alloys was recognized early-on [31]. While, in fluoride salt at 800 °C, maraging steel (12% Ni - 5% Cr - 3% Mo bal. Fe) and Hastelloy N showed corrosion rates of 14 μm/year and 1.5 μm/year respectively while the corrosion rate of SS304 was as high as 28 μm/year [31]. Chemical compositions of Hastelloy N (Alloy N, INCOR-8) and other Ni-base alloys, later developed for MSR structural material, are listed in the following Table 3.

Table 3. Chemical composition of the nickel-base alloys (wt.-%) [32, 33]

Element	ORNL Hastelloy N (INCOR-8)	ORNL Hastelloy N Ti-modified	ORNL Hastelloy N Nb-mod.	Czech Republic MONICR	Russia HN80M-VI	Russia HN80MTY (EK-50)	Russia HN80MT	France EM-721
Ni	Base	Base	Base	Base	Base	Base	Base	68.6
Cr	**7.52**	**6-8**	**6-8**	**6.85**	**7.61**	**6.81**	**7.02**	**5.7**
Mo	16.28	11-13	11-13	15.8	12.2	13.2	12.1	0.07
Ti	0.26	2	-	0.026	0.001	0.93	1.72	0.13
Fe	3.97	0.1	0.1	2.27	0.28	0.15	<0.33	0.05
Mn	0.52	0.15-0.25	0.15-0.25	0.037	0.22	0.013	<0.1	0.086
Nb	-	0-2	1-2	<0.01	1.48	0.01	-	-
Si	0.5	0.1	0.1	0.13	0.04	0.04	<0.05	0.065
Al	0.26	-	-	0.02	0.038	1.12	-	0.08
W	0.06	-	-	0.16	0.21	0.072	-	25.2
Cu	0.02	-	-	0.016	0.12	0.02	<0.01	-
Co	0.07	-	-	0.03	0.003	0.003	-	-
Ce	-	-	-	<0.003	0.003	0.003	-	-
Zr	-	-	-	0.075	-	-	-	-
B	<0.01	0.001	0.001	<0.003	0.008	0.003	<0.001	-
S	0.004	0.01	0.01	0.003	0.002	0.001	<0.001	-
P	0.007	0.01	0.01	0.003	0.002	0.002	<0.001	-
C	0.05	0.05	0.05	0.014	0.02	0.025	0.004	-

Suitable nickel-based alloys for MSR deployment are therefore characterized by low chromium concentration of 6-8 wt.%, high molybdenum contents of 11-16 wt.%, grain boundary

strengthening by the addition of 1-2 wt.% titanium or niobium, and minor amounts (0.01-0.008 wt.%) of boron. Suitable alloys also contain a low-degree of age hardening by the eventual addition of aluminum and copper, and low sub-wt.% content in solid-solution strengthening metals such as cobalt and tungsten. As an alternative, the French alloy EM-721 is a low-chromium, high-tungsten alloy, for achieving exceptionally high solid solution strengthening.

Since the very early days of the technological development of liquid fueled nuclear reactors, nickel-based alloys have been regarded as the containment material of choice because of their superior compatibility with corrosive media [34]. Early candidates such as Inconel, INOR-8 (later named Alloy N or Hastelloy N) or Hastelloy B (where Cr is replaced by Mo) were selected and tested using convection loop-type corrosion tests. Loop-type corrosion testing is still considered to be the standard method and provides the most accurate data generally free of artifacts. Later during the Molten Salt Reactor Experiment (MSRE) Ni-based Mo-Cr Hastelloy N (balance Ni, 15-17% Mo, 6-8% Cr, 4-6% Fe, 0.04-0.08% C) was specifically designed and optimized for low homogeneous corrosion rates in fluoride salt melts, low susceptibility for grain boundary embrittlement by fission tellurium (modified Hastelloy N by the addition of 1-2 wt.% Nb and/or Ti), high-temperature tolerance, and fairly low radiation-induced void swelling [6, 11]. Because of its high nickel content, Hastelloy N is a far more expensive material than stainless steel and not as readily available, but most importantly, it suffers from softening and decreased tensile properties at temperatures above 700 °C. Additionally, based on their face-centered cubic (fcc) crystal structure, Ni-based alloys show void swelling and tend to embrittle when exposed to core levels of neutron flux in excess of 10^{20} neutron/cm^2 even at temperatures as high as of 500 °C to 650 °C. Even though Hastelloy-N shows superior chemical compatibility with halide salt melts, it is not yet approved by the Nuclear Regulatory Commission (NRC) as nuclear structural material because of radiation embrittlement, irradiation void swelling, and its low strength at temperatures above 700 °C. Niobium-modified Hastelloy N has the best chances of any Ni-based alloy for NRC certification, but more supporting information on radiation embrittlement and irradiation induced void swelling must be generated. Hastelloy N is still considered for potential use as reactor vessel, core barrel, control rod system, piping and pumps in primary and secondary coolant loops, and as primary and secondary heat exchangers. For all Gen-IV nuclear reactor concepts, a design life of 60 years is required. Although some reactor components may be designed as replaceable structures, for operation and economic efficiency, continuous long-term services are highly desired.

Unfortunately, efforts on improving Hastelloy N did not continue to reach any definitive conclusions before the MSRE project was terminated. To eventually achieve a mature Hastelloy N variant with improved properties for the current MSR development and deployment, the efforts must be resumed with an extensive research campaign [33]. Besides Hastelloy N variants that are mainly focused on addressing radiation (He) embrittlement issues must also be developed for service at higher temperatures. Therefore, new nickel-based low chromium high-temperature alloys have been developed in recent years which could very well provide a valid alternative to Hastelloy N for molten salt applications. Haynes 244, which is improved over Haynes 242, could be considered as a strong candidate for molten salt applications, since it shows mostly enhanced high-temperature mechanical properties compared with Hastelloy N (Table 4, and Table 5). Sufficient experimental data on the chemical compatibility of Haynes 244 in molten salts is not available to date.

Table 4. Brief description of Ni-Cr-Mo alloys Hastelloy N and Haynes 244

	Nickel-based Alloys suitable for molten salt environments
Hastelloy N UNS N10003	**Ni 71 Mo 16 Cr 7 Fe 5 max. Si 1 max. Mn 0.8 max. W 0.5 max. Al+Ti 0.5 max. Cu 0.35 max. Co 0.2 max C 0.08 max.** Hastelloy N alloy is a nickel-base alloy developed at Oak Ridge National Laboratories as container material for molten fluoride salts. It is sold solution strengthened combined with γ'-Ni_3(Al,Ti) based precipitation hardening. It has good oxidation resistance to hot fluoride salts in the temperature range of 704 to 871°C. In tests of over two years duration, corrosion attack in molten fluoride salts at temperatures up to 704 °C, was less than 25 μm per year. Hastelloy N alloy has good oxidation resistance in air. It shows promise for continuous operations at temperatures up to 982 °C. Intermittent use at temperatures up to 1900 °F (1038 °C) may also be possible. No discernible oxidation could be measured for the alloy at temperatures up to 649 °C.
Haynes 242 UNS N10242	**Ni bal. Mo 25 Cr Fe 2 max. Co 1 max. Mn 0.8 max. Al 0.5 max. C 0.03 max. B 0.006 max.** Haynes 242 (UNS N10242) is an age-hardenable nickel-molybdenum chromium alloy which derives its strength from a long-range ordering reaction upon aging. It has tensile and creep strength properties up to 649-704 °C which are as much as double those for solid solution strengthened alloys, but with high ductility in the aged condition. The thermal expansion characteristics of the 242 alloy are much lower than those for most other alloys, and it has very good oxidation resistance up to 816 °C. Other attractive features include excellent low cycle fatigue properties, very good thermal stability, and resistance to high-temperature fluorine and fluoride environments. Haynes 244 has been developed as an upgrade from Alloy 242, with enhanced tensile and creep properties up to 760 °C, as well as a lower coefficient of thermal expansion.
Haynes 244	**Ni 70 min. Mo 22.5 Cr 7 W 6 Fe 2 max. Mn 0.8 max. Al 0.5 max. C 0.03 max.** Haynes 244 is a Ni-Mo-Cr-W alloy developed for static parts in advanced gas turbine engines which require low thermal expansion at temperatures up to 760 °C. The alloy is age-hardenable by the formation of Ni_2(Cr,Mo,W) domains, which are structurally similar to the strengthening domains in Haynes 242. Alloying with tungsten increased the thermal stability of these domains and lowers the coefficient of thermal expansion. Other important properties such as oxidation resistance and low-cycle fatigue performance are comparable or better than those of Haynes 242.

Table 5. Basic mechanical room temperature properties of Hastelloy N and Haynes 244

Alloy and Properties	0.2% Yield Strength (MPa)	Ultimate Strength (MPa)	Elongation	Thermal Expansion (μm/mK)	Youngs Modulus (GPa)	References
Hastelloy N UNS N10003	275	800	0.39	12.3 @ 21-316°C	219	Azom.com Hpalloys.com
Haynes 242 UNS N10242 Solution annealed and aged	760	1235	0.44	11.6@25-300°C 15@ 25 - 1000°C	229	Matweb.com Haynesintl.com
Haynes 244 Solution annealed and aged	902	1414	0.296	11.2 @ 25-300°C 13.8 @ 25-800°C	223	Haynesintl.com

The commercial alloys Haynes 242 (UNS N10242) and Haynes 244 might be seriously considered for MSR applications in addition to Hastelloy N and its modified derivatives. Haynes 242 is a nickel-based age-hardenable alloy mainly containing 25Mo-8Cr-Fe-Co, has good tensile and creep strength properties up to 705 °C with low thermal expansion and high resistance to high-temperature halide environments (Haynes international). The alloy is code qualified for ASME BPVC Section VIII Division 1 to 538°C [33]. Some tensile and creep data exist that could provide a foundation for further nuclear codification. However, based on the limited data available, the high-temperature properties of Haynes 242 do not seem to have significant advantages over those of Hastelloy N. Haynes 244, on the other hand, is an upgraded alloy over Haynes 242. Haynes 244 is also a nickel-based age-hardenable alloy mainly containing 22.5Mo-8Cr-6W-Fe with good tensile strength properties up to 760 °C with low thermal expansion. Limited data suggests that Haynes 244 possesses better high-temperature capabilities, including creep strength, compared with Haynes 242. Alloy 244 is age-hardenable by formation of Ni_2(Cr,Mo,W) domains, which are structurally similar to the strengthening domains in alloy 242. Alloying with tungsten increases the thermal stability of these domains and further lower the coefficient of thermal expansion of Haynes 244 over Haynes 242. Other important properties such as oxidation resistance and low-cycle fatigue performance are comparable or even better than those of Alloy 242 (Figures 15-17).

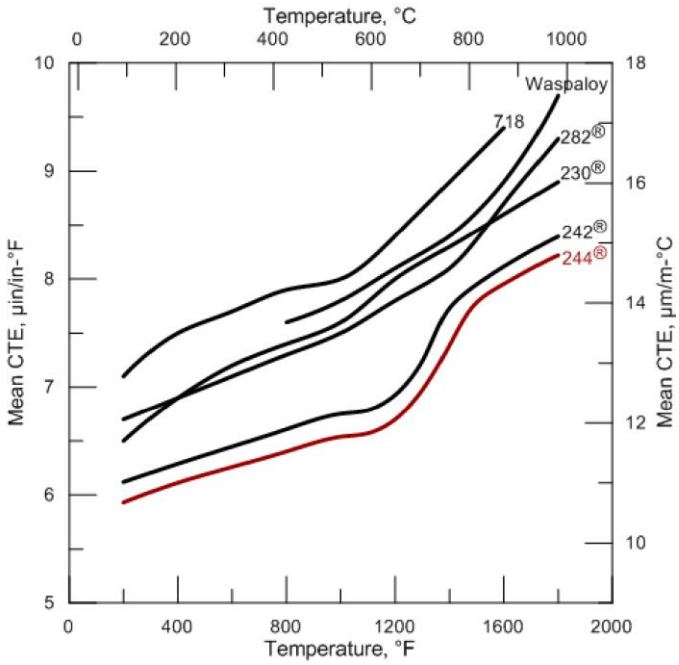

Figure 14. Coefficient of thermal expansion of Haynes 242 and 244 compared with other superalloys [35]

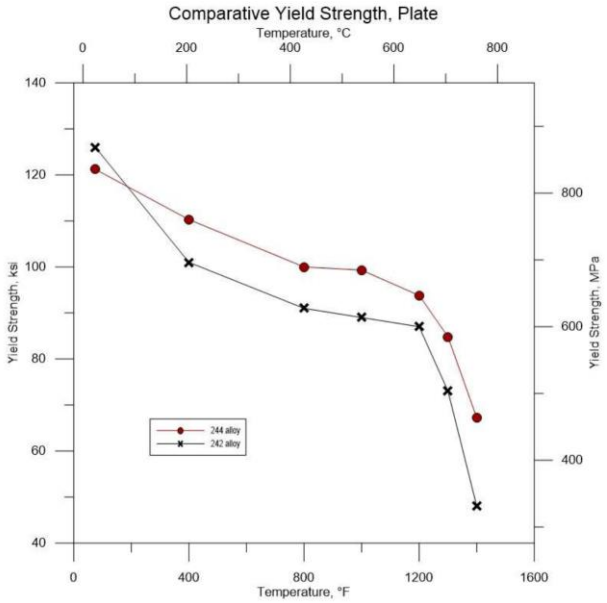

Figure 15. Yield strength of Haynes 244 compared with Haynes 242 [35]

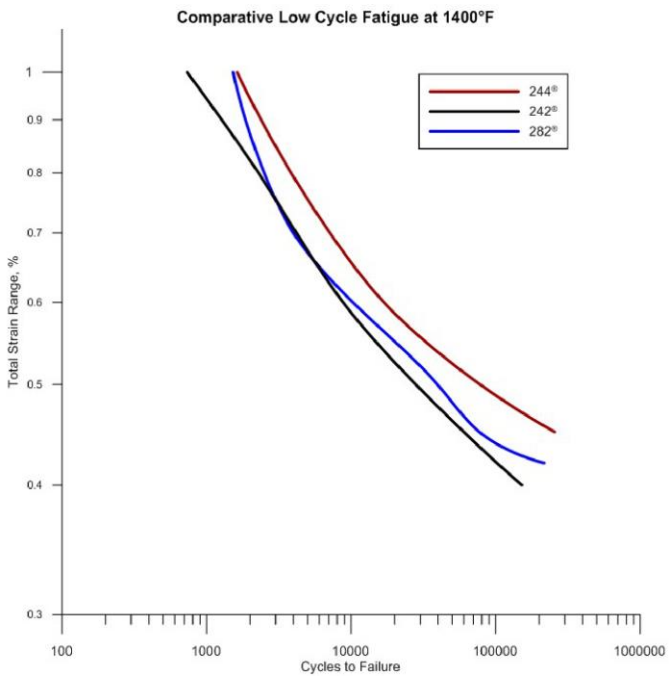

Figure 16. Low cycle fatigue of Haynes 242, 244, and 282 at 760 °C (1400 F) [35]

1.8 Constituency and properties of high-temperature alloys and superalloys

In this section the make-up and properties of the most prominent commercial superalloys for high temperature deployment are evaluated. The aim is to provide a comparison between each superalloy to further define their fundamental difference as compared to MSR alloy candidates.

The following table provides a brief look at the properties of the individual alloying metals. In this table, the properties of alloying metals are compared against nickel as the prominent solid solution matrix (Table 6).

Table 6. Physio-mechanical properties of alloying metals

Property /Element	V	Cr	Mn	Co	Ni	Nb	Mo	Ta	W	Re	Os	Ir
Density ρ (g/cm^3)	6.1	7.14	7.47	8.9	8.9	8.57	10.28	16.65	19.25	21.02	22.6	22.65
Melting point T_m (K)	3183	2180	1519	1768	1728	2750	2896	3290	3695	3459	3306	2739
Enthalpy (kJ/mol)	514.2	396.6	280.7	424.7	429.7	725.9	658.7	782	849.2	769.9	791.0	665.3
Atomic Radius (pm)	135	140	140	135	135	145	145	145	135	135	130	135
Crystal class	Im-3m	Im-3m	I-43m	$P6_3$/mmc	Fm-3m	Im-3m	Im-3m	Im-3m	Im-3m	$P6_3$/mmc	$P6_3$/mmc	Fm-3m
Abundance in crustal rock (ppm)	190	140	1100	30	90	17	1.1	1.7	1.1	0.0026	0.0018	0.00004
Youngs Modulus (GPa)	128	279	198	209	200	105	329	186	411	463	560	528
Shear Modulus (GPa)	47	115	76.4	75	76	38	20	69	161	178	222	210
Brinell /Vickers Hardness (MN/m^2)	628/ 628	1120 1060	196/ 500	700/ 1043	700/ 638	736/ 1320	1500 1530	800/ 873	2570 3430	1320 2450	3920 /670	1670 1760
Strength. Constant K_1 (MPa $at\%^{1/2}$)	408	337	448	39.4	NA	1183	1015	1191	977	ND	ND	ND

Strengthening constant K_1 was used from [28] based on equation (2)

Bulk properties were extracted from http://webelements.com and https://www.matweb.com

As the data suggests, molybdenum and tungsten are obvious candidates to improve high-temperature strength of nickel-based superalloys due to their significant impact to solid-solution strengthening. Both metals exhibit high melting temperatures, large enthalpies, high Youngs moduli, high hardness, and fairly high strengthening constants. Based on this data, a silver-bullet alloy formulation, however, cannot be derived. Molybdenum shows a low shear modulus, rhenium (Re) and osmium (Os) have very high melting temperatures, high enthalpies, high

Youngs- and shear moduli, and high hardness, but are prohibitively scarce and expensive. Tantalum (Ta) and Niobium (Nb) show the highest strengthening constants but are only used for precipitation hardening and enhancing grain boundary strength in concentration of up to 3 wt.%. The use of Manganese (Mn) at a high concentration might be justified solely for economic reasons because of its high abundance in the earth's crust. Its use as constituent for high temperature super alloys, however, is very restricted due to its low melting temperature, low enthalpy, low Youngs and shear moduli, low hardness, and below average strengthening constant.

1.8.1 Common nickel-based high-temperature alloys

In the following table an overview of some commercially available nickel-based high-temperature alloys and superalloys is provided (Tables 7). This overview shows a selection of commercial superalloys which is by no means complete.

Table 7. Common nickel-based high temperature alloys and superalloys

	Nickel-based high-temperature alloys and superalloys
A-286 **UNS S66286**	**Ni 24-27 Cr 14-16 Mo 1-1.5 Si 1 Ti 1.9-2.35 Al 0.35 V 0.1-0.5 Mn 2 B 0.003-0.01 Fe bal.** A-286 is a nickel and iron-based high-temperature alloy similar to austenitic stainless-steel with high oxidation resistance, high strength, good stress rupture qualities. It is age-hardeneable and is used for applications requiring high strength and corrosion resistance. It can maintain high strength with continuous exposure from -190 to 700°C and remains resistant to oxidation when continuously exposed to 815°C and intermitted temperatures of 980°C.
Hastelloy X **UNS N06002**	**Ni 47 min. Cr 22 Fe 18 Mo 9 Co 1.5 W 0.6 Mn 1 max. Si 1 max. Nb 0.5 max. Al 0.5 max. Ti 0.15 max.** Hastelloy X is a nickel-chromium-iron-molybdenum alloy that possesses an exceptional combination of oxidation resistance, fabricability and high-temperature strength. It has also been found to be exceptionally resistant to stress-corrosion cracking in petrochemical applications. X alloy exhibits good ductility after prolonged exposure at temperatures of 650, 760 and 870 °C for 16,000 hours. Good resistance to oxidation, good resistance to atmospheres of up to 1200 °C, high corrosion resistance, excellent forming, and welding qualities. Hastelloy X has ASME Boiler and Pressure Vessel code case.
Haynes 230 **UNS N06230**	**Ni 57, Cr 20-24 W 13-15 Mo 1-3 Co 5 max Fe 3 max. Mn 0.3-1 Si 0.25-0.75 Al 0.2-0.5 La 0.005-0.05** Haynes 230 is a solid solution-strengthened nickel-chromium-tungsten-molybdenum alloy that combines excellent high temperature strength, outstanding resistance to oxidizing environments up to 1150 °C for prolonged exposures, premier resistance to nitriding environments, and excellent long-term thermal stability. This alloy has good fabricability at room temperature, is castable, and is particularly effective for very long-term applications at temperatures of 650 °C. Other attractive features include lower thermal

	expansion characteristics than most high-temperature alloys, and a pronounced resistance to grain coarsening with prolonged exposure to high-temperatures.
Inconel 600 **UNS N06600**	**Ni 76.0, Cr 15.5, Fe 8.0** Inconel 600 is a high temperature high nickel, high chromium alloy showing good resistance to oxidizing, reducing, and severely corrosive environments at elevated temperatures. It has good oxidation resistance at up to 635 °C. It is often used for furnace muffles, electronic components, chemical and food processing equipment, heat treating equipment, and nuclear steam generator tubing. It has high strength, good resistance to corrosion, good formability, and good hot and cold workability.
Inconel 601 **UNS N06601**	**Ni 61 Cr 23 C 0.10 Mn 1.0 Al 1.4 Fe bal. S 0.015 Si 0.5** Inconel 601 has high nickel and chromium content for better resistance to oxidizing and reducing environments. It is suitable for severely corrosive environments at elevated temperatures. It has good oxidation resistance to 650 °C and good formability. Inconel 601 is used for instrument probes, furnace muffles, electronic components, chemical and food processing equipment, heat treating equipment, nuclear steam generator tubing.
Inconel 617 **UNS N06617**	**Ni 44.5 min. Cr 20-24 Co 10-15 Mo 8-10 Al 0.8-1.5 Fe 3 max. Si 1 max. Ti 0.6 max.** See section 1.3, page 7.
Inconel 625 **UNS N06625**	**Ni 58 min. Cr 20-23 Mo 8-10 Nb 3.15-4.15 Fe 5 max.** See section 1.3, page 7.
Waspaloy **Alloy 685** **UNS N07001**	**Ni 52 min. Cr 18-21 Co 12-15 Mo 3.5-5 Ti 2.75-3.5 Fe 2 max. Al 1.2-1.6 B 0.003-0.01** Alloy 685 shows high strength, high oxidation resistance, difficult weldability, and better creep-rupture strength than the Inconel 718. Waspaloy is an age-hardening nickel-based high-temperature alloy. The hardening and strength properties are developed by precipitation of γ'-Ni_3(Ti,Al). The solution temperature is between 1032-1043 °C which is also the grain growth temperature. Water quenching will result in Rockwell hardness values of B 90 or higher. Its best stress rupture and creep properties are obtained by solution annealing at 1038-1079 °C. It is commonly used for applications that encounter extreme environments. It's very high strength at elevated temperatures is generally comparable to that of Rene 41 and superior to Inconel 718. It is used for gas turbine engine parts, aerospace components, springs, and fasteners.

Rene 41 **UNS N07041**	**Ni 47 min. Cr 18-20 Co 10-12 Mo 9-10.5 Fe 5 max. Ti 3-3.3 Al 1.4-1.6 B 0.003-0.01** Rene 41 is a precipitation hardening, nickel-chromium-cobalt based high temperature alloy possessing high strength in the 649 to 982 °C temperature range. This alloy is sensitive to strain age cracking during welding and designed for use in severely stressed high temperature applications where it shows exceptional oxidation resistance. It is commonly used in applications where extreme temperatures are encountered and high strength is required. Mechanical properties vary with the solution and aging treatments. Higher solution temperatures result in better room temperature ductility and elevated temperature creep-rupture strength. Lower solution temperatures give higher tensile strengths.
Inconel 718 **UNS N07718**	**Ni 50-55 Cr 17.0-21 Mo 2.8-3.3 Nb+Ta 4.75-5.5, Ti 0.65-1-15 Al 0.2-0.8 Co 1 max. Fe bal.** Inconel 718 is a precipitation hardenable nickel-chromium alloy that has high creep-rupture strength at high temperatures up to 700 °C. The poor age-hardening response of alloy 718 permits annealing and welding without spontaneous hardening during heating and cooling. This alloy has excellent weldability compared to the nickel-base super alloys hardened by aluminum and titanium. Alloy 718 shows excellent strength from -250 °C to 700 °C, is age hardenable and may be welded in fully aged condition. It shows excellent oxidation resistance at up to 980 °C. It is used for jet engines, pump bodies and parts, rocket motors and thrust reversers, nuclear fuel element spacers, and hot extrusion tooling. Alloy 718 has outstanding resistance to post weld cracking, good tensile strength, good rupture strength, good fatigue strength. Inconel 718's ease of production has allowed it to become mainstream in a large number of applications.
Inconel 725 **UNS N07725**	**Ni 55-59 Cr 19.0-22.5 Mo 7-9.5 Nb 2.75-4 Ti 1-1.7 Fe bal.** Inconel 725 is a nickel-chromium-molybdenum-niobium alloy that is highly resistant to corrosion and is age hardenable for extremely high strength. It has essentially the same corrosion resistance as alloy 625, which is widely used in a broad range of severely corrosive environments. Alloy 725 is deployed across several industries. Alloy 725 is chosen over alloy 625 when higher strength is required. The strength of age-hardened Inconel 725 is far higher than that of annealed alloy 625. Because the strength of alloy 725 is developed by heat treatment not by cold work, its ductility and durability remain high. Also, the alloy's strength can be imparted to large or non-uniform sections that cannot be strengthened by cold work.
Inconel X-750 **UNS N07750**	**Ni 70 min. Cr 14-17 Fe 7-9 Ti 2.25-2.75 Al 0.4-1 Nb+Ta 0.7-1 Mn 1 max. Co 1 max.** Inconel X-750 has good corrosion resistance, good oxidation resistance, high tensile strength, is non-magnetic, and has high temperature resistance up to 700 °C. Inconel X-750 is a precipitation-hardenable nickel-chromium alloy with high strength at temperatures up to 704°C. Although much of the effect of precipitation hardening is lost with temperatures over 704 °C, the heat-treated material has useful strength up to 982 °C. Alloy X-750 also has excellent

	properties down to cryogenic temperatures. This nickel-chromium based alloy is similar to Inconel 600 but is precipitation-hardeneable due to the addition of titanium and aluminum.
Haynes Alloy 25 **UNS R30605**	**Co 51 bal. Cr 20.0, W 15.0, Ni 10.0, Fe 3.0 max. Mn 1.5 Mo 1 max Si 0. 4 max.** Alloy 25 is a solution strengthened cobalt-chromium-tungsten alloy showing excellent strength for continuous service at 980 °C. It is oxidation and carburization resistance at up to 1038 °C, and galling resistant. It has demonstrated resistance to marine environments, acids, and body fluids. Alloy 25 is non-magnetic, even when severely cold reduced. It can reach Rockwell C hardness of 50 when cold reduced and aged. Alloy 25 is resistant to hydrochloric and nitric acid at certain concentrations and temperatures, and wet chlorine environments at room temperature. It is used for gas turbine engine components such as combustion chambers, and afterburners. Other uses also include high temperature ball bearing service, springs, and heart valves.
Haynes 188 **UNS R30188**	**Co 39 min. Cr 22 Ni 22 W 14 Fe 3 Mn 1.25 max. Si 0.35 La 0.03 B 0.015 max** Haynes 188 is a cobalt-chromium-nickel-tungsten alloy with high-temperature strength, good oxidation resistance, high corrosion resistance, good forming and welding properties. Haynes 188 is a solid solution-strengthened alloy that combines excellent high-temperature strength with very good resistance to oxidizing environments at up to 1095 °C for prolonged exposures, and excellent resistance to sulfate deposit hot corrosion. It is readily fabricated and formed by conventional techniques and has been used for cast components. Other attractive features include excellent resistance to molten chloride salts, and good resistance to gaseous sulfidation. The high-temperature alloy possesses characteristics that allow it to be widely used in the aerospace market.

References: Ulrich.com, ASM.matweb.com, Haynesintl.com, Spacematdb.com, Specialmetals.com, Hpalloys.com, Hightempmetals.com, Carpentertechnology.com, Alloywire.com

The 14 introduced nickel-based high-temperature alloys and superalloys can be grouped into one of the following six categories:

- **Ni-Cr-Fe** such as A-286, Alloys 600, 601, and alloy X-750

Alloy A-286 and Inconel X-750 will undergo age hardening and precipitation strengthening while Inconel 600 and 601 are used for their excellent high-temperature corrosion resistance and workability but can only be hardened through cold work.

- **Ni-Cr-Fe-Mo** such as Hastelloy X

Hastelloy X is mainly a solid-solution strengthened alloy with good ductility after long-exposure to high temperatures and shows therefore excellent resistance to corrosion fatigue and stress-corrosion cracking.

- **Ni-Cr-Mo-Nb** such as Alloys 625, 718, and 725

These alloys combining solid solution hardening with age hardening and precipitation strengthening. Alloy 725 can be strengthened to higher degree compared with 625. Alloy 718 is precipitation hardenable but shows poor responds to age hardening. All have excellent oxidation resistance and better weldability than Al-Ti hardened Ni-based superalloys.

- **Ni-Cr-W-Mo** such as Haynes 230

Haynes 230 is a solid-solution hardened superalloy with outstanding high-temperature strength and particularly suited for long-term application at temperatures above 650°C without the risk of crack-corrosion and maintains ductility.

- **Ni-Cr-Co-Mo** such as Inconel 617, Waspaloy, Rene 41

While Inconel 617 is basically a solution strengthened alloy with γ'-Ni_3(Ti,Al) precipitation in the temperature range 500-900°C, the properties of Waspaloy and Rene 41 are derived mainly by precipitation strengthening and the formation of γ'-Ni_3(Ti,Al). The superior high-temperature strength of Waspaloy and Rene 41, compared with Inconel 718, provides them excellent creep propertied, but makes them susceptible to stress corrosion.

- **Co-Ni-Cr-W** such as Haynes 25 and Haynes 188

The solid-solution strengthened cobalt-based superalloys Haynes 25 and 188 have been developed for extreme high temperature strength and superior creep resistance, and continues service in oxidizing environments at 980 °C. They have good resistance to molten chloride salts.

1.8.2 Properties of nickel-based superalloys in comparison

In the following section room-temperature properties of the 14 previously described nickel-based alloys and superalloys are compared (Table 8).

Table 8. Mechanical room temperature properties of 14 nickel-based alloys and superalloys

Alloy and Properties	0.2% Yield Strength (MPa)	Ultimate Strength (MPa)	Elongation	Hardness	Youngs Modulus (GPa)	Shear Modulus (GPa)	References
Alloy 286 Solution annealed	275	620	0.40	85 Rockwell B	201	77	Upmet.com ASM.matweb.com
Hastelloy X	379.2	758	0.44	96 Rockwell B	205	77.9	Hpalloy.com ASM.metweb.com

							Spacematdb.com
Haynes 230 Plate annealed	383	852	0.46	100 Rockwell B	209	79	Ulbrich.com Haynesintl.com
Inconel 600 Plate annealed	205-345	550-752	0.35-0.55	65-85 Rockwell B	214	80.8	Specialmetals.com
Inconel 601 Plate rolled annealed	450	760	0.42	65-75 Rockwell B	206.5	81.2	Techsteel.net Specialmetals.com Hpalloys.com
Inconel 617 Plate rolled annealed	322	734	0.62	87-88 Rockwell B	211	81	Specialmetals.com Hightempmetals.com
Inconel 625 Plate annealed	462	896	0.44	98 Rockwell B	208	81.2	Hightempmetals.com
Waspaloy Alloy 685 Bar anneal	980	1358	0.30	42 Rockwell C	211	81	Carpentertechnology.com Specialmetals.com
Rene 41 Plates rolled annealed	820	1262	0.21	33-40 Rockwell C	218	83	Rolledalloys.com Alloywire.com
Inconel 718 Plate annealed	414	827	0.3	34-44 Rockwell C	200	80	Ulbrich.com
Inconel 725 Age hardened	892	1254	0.32	36-37 Rockwell C	204	78	Specialmetals.com
Inconel X-750	724	1137	0.20	34-40	214	75.8	Alloywire.com Sprcialmetals.com

				Rockwell C			
Haynes 25 Plate Solution annealed	474	1000	0.59	99 Rockwell B	225	ND	Hpalloys.com Haynesintl.com Hightempmetals.com
Haynes 188 Plates solution annealed	483	982	0.51	98 Rockwell B	232	90	Haynesintl.com Ulrich.com Alltempalloys.com

Room-temperature properties of the selected high-temperature alloys and superalloys do vary based on shape (sheet, plate, bar), heat treatment, cold-work, microstructure, grain-size (Hall-Petch relationship), and annealing. Therefore, a fair comparison is not a simple task. We intend to compare the alloys by preferably using data on solution annealed plate material. Within this comparison, the basic mechanical properties such as the modulus of elasticity (Young's Modulus) and the shear modulus vary greatly considering the different nature of the alloys. For example, the Youngs modulus varies between 200 GPa (Inconel 718) and 232 GPa (Haynes 188) and the shear modulus between 77 GPa (Alloy 286) and 90 GPa (Haynes 188). On the other hand, yield strength, ultimate strength, elongation, and hardness do show large variations and cover a wide property window.

The combination of solid solution strengthening and precipitation hardening (age hardening) lead to the highest values on 0.2% yield strength and ultimate strength. Waspaloy, Rene 41, Inconel 725, and Inconel X-750 show ultimate strength in excess of 1100 GPa and yield strengths larger than 700 GPa. These high strength values are associated with high hardness values around 40 Rockwell C, but consequently also exhibit low ductility and elongations as low 20 % to 32 %. Besides of their excellent creep strength to up to 1000 °C, these high-strength superalloys might show a tendency for high-temperature cracking and stress corrosion cracking. The strength of these alloys is derived by the formation of γ'-$Ni_3(Ti,Al)$ during deployment at high temperatures, and the precipitation of primary and secondary carbides $M_{23}C_6$, and M_6C, and MC, in addition to the strength of the solid solution γ-phase.

A good example of solid solution strengthening is provided by the cobalt-based (Co-Cr-W-Ni) superalloys Haynes 25 and Haynes 188, as well as the tungsten-based (Ni-Cr-W-Mo) Haynes 230, which combine outstanding creep resistance and high-temperature strength with fairly good ductility. The ultimate strength of these solution strengthened alloys is between 852 GPa (Haynes 230) and 1000 GPa (Haynes 25) with high values for elongation of 46 % (Haynes 230) to 59 % (Haynes 25).

1.8.3 High-temperature properties of nickel-based alloys and superalloys

In the following section, the high temperature properties, and high-temperature performance of nickel-based high-temperature alloys such as Haynes 25, 188 and 230 are compared with those of Inconel 600 and 625, and Hastelloy X. This comparison is somewhat relevant since it provides a better understanding on the additional effect of precipitation strengthening (Inconel 625, 617) compared with only solid solution strengthening (Haynes 25, 188, 230 and Hastelloy

X). Haynes alloys exhibit excellent low cycle fatigue properties at elevated temperature. (Figure 17).

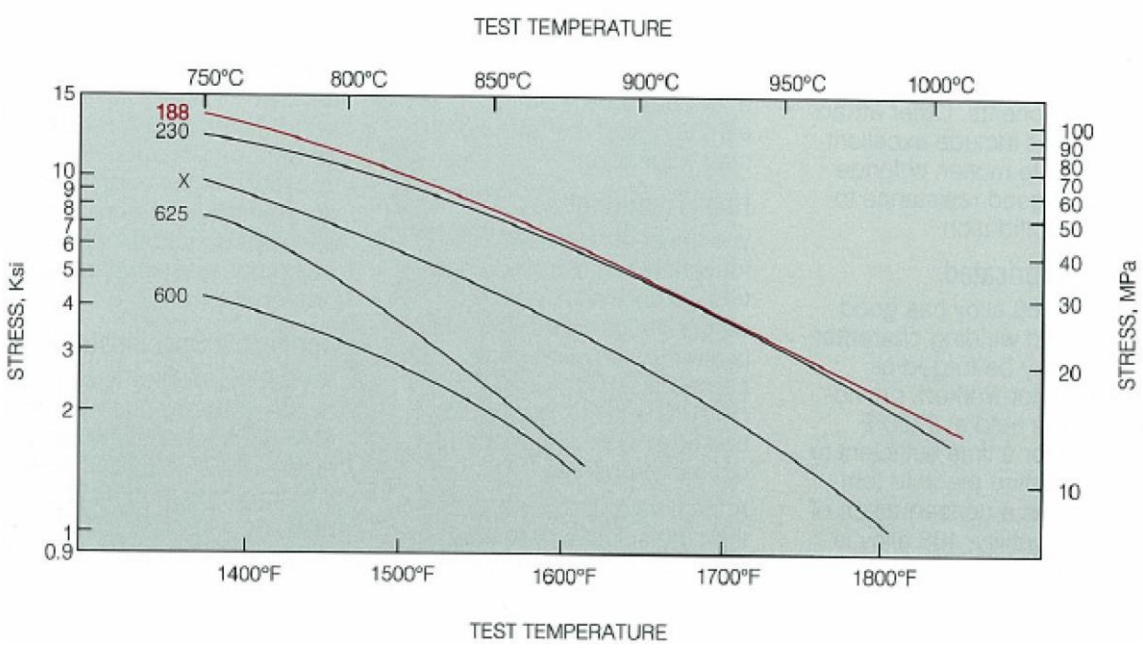

Figure 17. Comparison of stress to produce 1 % creep in 1000 Hours at temperatures of up to 1800 °F (982 °C) (Sheet, Haynesintl.com) [36, 37]

Stress rupture properties of solution-strengthened Haynes 230 reaches a maximum at about 870 °C. Haynes 230 performs worse than Inconel 625 at 760°C, but far better than Inconel 625 at higher temperatures (Table 9).

Table 9. Stress rupture properties of high-temperature alloys between 760-982 °C [36]

Alloy	760°C 103 MPa	871°C 31 MPa	982°C 14 MPa
230	**8,200**	**65,000**	**5,000**
625	19,000	14,000	2,400
X	900	5,000	2,100
800H	130	1,200	920
INCONEL 601	50	1,200	1,000
253 MA	140	900	720
600	15	280	580
316 SS	100	240	130
RA330	30	230	130

304 SS	10	100	72

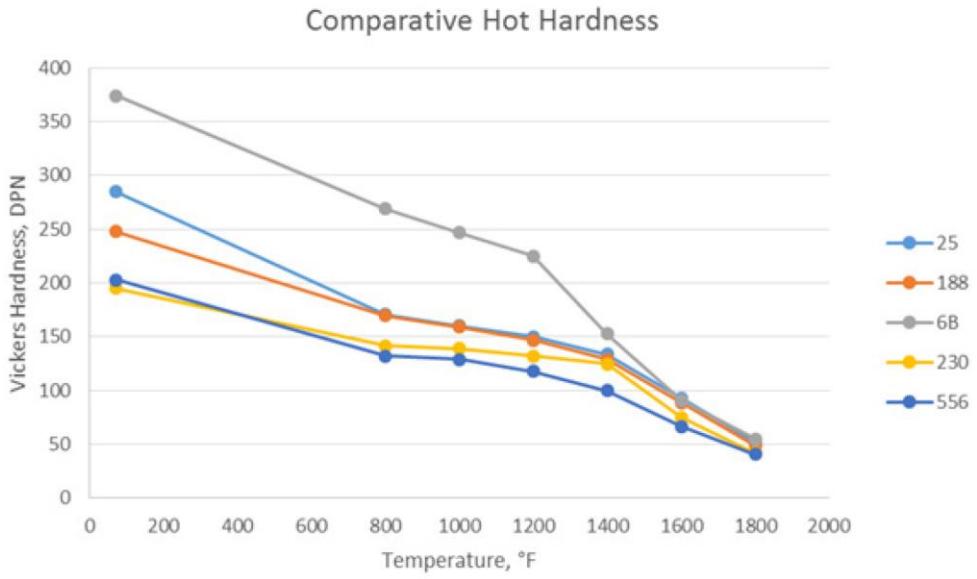

Figure 18. High-temperature Vickers Hardness of Haynes 25, 188 and 230 at temperatures of up to 1800 °F (982 °C) (Haynesintl.com) [36, 37]

Haynes 25, 188, and 230 all show overall excellent high-temperature Vickers hardness (Figure 18). Vickers hardness does decline in an approximately nearly linear manner with temperature until 760° (1400 °F) and then shows a steeper drop until 982 °C (1800 °F). While at those high temperatures the Haynes alloys show about the same hardness. However, at lower temperatures, Alloy 25 performs better than 188 which performs better than 230. The Haynes alloy 230 shows excellent retained ductility after long-term thermal exposure at intermediate temperatures (Figure 19). It does not exhibit chromium-rich (sigma) σ-phase, (mu) μ-phases such as W_6Co_7, Mo_6Co_7, W_6Fe_7 and Mo_6Fe_7 or metastable Ni_7Mo_6, or other deleterious phase formation even after 16,000 hours of exposure at temperatures from 649 to 871 °C. Principal phases precipitated from the solid solution in Haynes 230 are mainly all defined by carbides. In contrast, in other solid solution strengthened alloys such as Haynes 188, Inconel 625, and Hastelloy X some deleterious phase precipitation (Co_2W Laves phase) was observed, which did impact ductility, as well as tensile and impact strength.

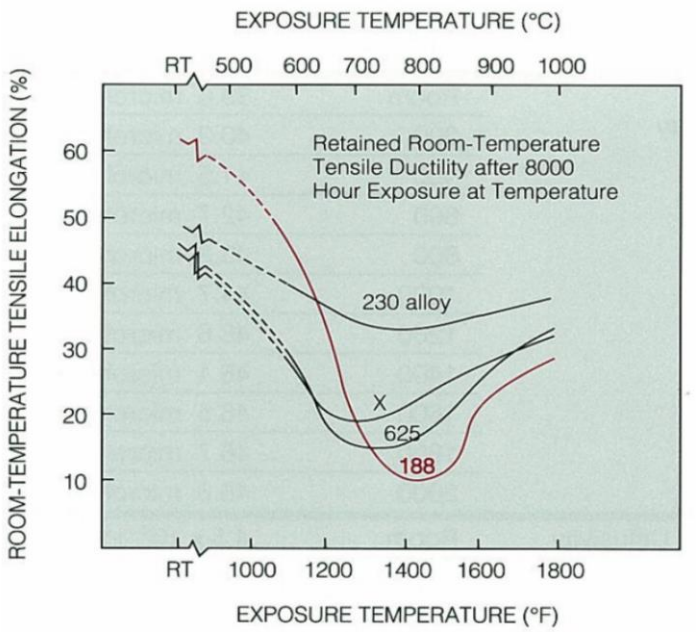

Figure 19. Room-temperature properties of plates of Haynes 230 and 188 compared with Hastelloy X and Inconel 625 after exposure to temperatures of up to 1800 °F (982 °C) (Haynesintl.com) [36, 37]

The Haynes alloys 188 and 230 exhibit excellent low cycle fatigue properties at elevated temperature, between 425 to 980 °C. Low cycle fatigue lives of Haynes 188 & 230, Hastelloy X, and Inconel 617 & 625 were tested at 427 °C and as-received alloys were compared with aged alloys annealed at 760 °C for 100 hours (Figure 20). Samples were machined from plate or bar. A test frequency of 0.33 Hz was used.

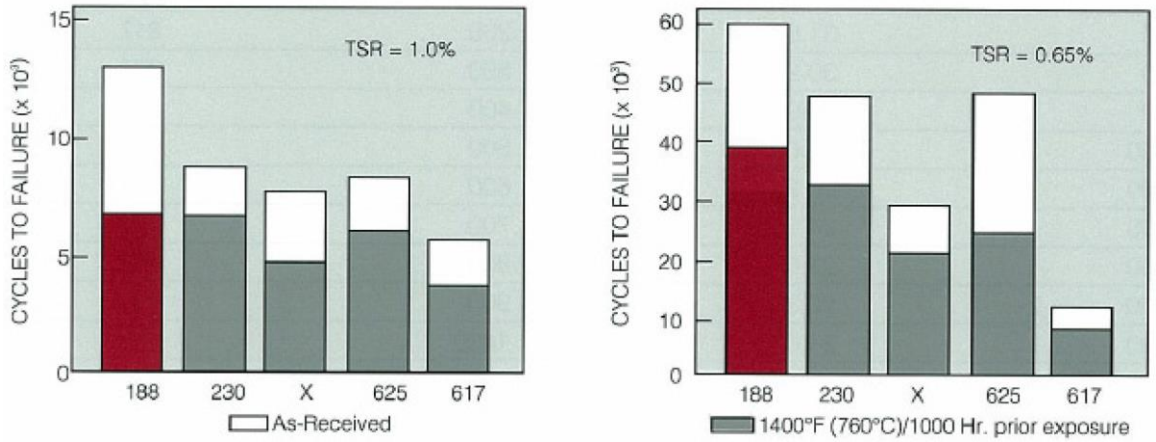

Figure 20. Low cycle fatigue lives at 425 °C of Haynes 188 and 230 compared with Hastelloy X, and Inconel 625 and 617. Left: as-received and right: after 1000 hours at 760°C. (Haynesintl.com) [36, 37]

Within this comparison among Haynes 25, 188 and 230, Inconel 600, 617, and 625, and Hastelloy X, information on high-temperature creep, hardness, elongation, and low cycle fatigue are provided [36] and are further used to aid the formulation of alternative nickel-based high-temperature alloy compositions. The Haynes alloys are solid-solution-strengthened combining excellent high-temperature strength with good fabricability at room temperature. Haynes alloys show outstanding performance in very long-term applications at temperatures of 650 °C or more. They are stronger than nickel-base solid-solution-strengthened alloys, and significantly stronger than simple nickel chromium or iron-nickel-chromium heat-resistant alloys. This fact could allow for significant thickness and weight reduction at superior design strength and service life.

Haynes 188 together with similar solution-strengthened superalloys such as Inconel 625, and Hastelloy X do show precipitation of deleterious phases after long-term exposure at elevated temperature. As an example, the formation of Co_2W Laves phases observed in Haynes 188 impairs impact strength and tensile ductility. In this regard, the behavior of Haynes 188 is much improved over Haynes 25 which it replaces. However, for applications where thermal stability has high importance the use of Haynes 230 is recommended to avoid the formation of Co_2W laves phases.

1.8.4 High-temperature corrosion resistance Haynes and Inconel

The high-temperature corrosion properties of nickel-based alloys and superalloys are compared (Table 10).

Table 10. Oxidation resistance after 1000 hours in flowing air between 980 °C and 1150 °C

Alloy	980°C		1095°C		1150°C	
	Metal affected (µm)	Metal Loss (µm)	Metal affected (µm)	Metal Loss (µm)	Metal affected (µm)	Metal Loss (µm)
188	28	3	94	13	272	218
230®	38	5	84	13	112	30
X	38	5	112	33	115	91
625	48	10	198	89	513	465
617	51	8	97	15	132	25

Haynes 230, Hastelloy X, and Inconel 617 do show excellent high temperature oxidation resistance under air flow (213 mm/min) at temperatures between 980 °C and 1150 °C, and low effective metal penetration depths at 1150 °C of 112 µm to 132 µm (Hynes 230) have been confirmed after 1000-hour test intervals. Haynes 188 and Inconel 625 showed lower performance with 272 µm and 513 µm under similar conditions.

Furthermore, Haynes 188 and 230, together with Inconel 625 and Hastelloy X show excellent high-temperature corrosion resistance in this comparison (Table 11). Their corrosion resistance at high temperature is somewhat better than of Inconel 617. The superior alloy here is Haynes 214, a nickel-chromium-aluminum-iron alloy which was developed to provide an optimum in high-temperature oxidation resistance for austenitic materials for uses at 955 °C or above [38]. Haynes 214 in this context exhibits resistance to oxidation far better than nearly all conventional heat-resistant wrought alloys. This extreme high-temperature oxidation resistance is attributable to the formation of a passivating adherent Al_2O_3-type oxide scale, which forms in preference to chromium oxide scales at high temperatures. At temperatures below 955 °C the alloy develops a somewhat less dense oxide scale which is a mixture of chromium and aluminum oxides. The Al_2O_3-type scale at higher temperatures provides the alloy with excellent resistance to carburization, nitriding, and corrosion in chlorine-bearing oxidizing environments [38].

Table 11. Water vapor oxidation (air with 20 % water) of nickel-based alloys after 1008 hours at 982 °C [37]

Alloy	Metal Loss (µm)	Average Metal Affected (µm)
214	1	16
230	5	40
625	9	42
188	**5**	**38**
X	7	45
617	10	50
556	9	47
HR-120	10	53
800HT	63	129

2.0 Experimental

We have developed experiments to determine diffusivity of alloying metals in SS316, Inconel 625 and 617 and to allow for the speciation of corrosion products on alloy foil material. Our approach employs a wide range of experimental research, bridging chemical analysis and speciation of corrosion products with imaging and solid-state materials chemistry with high spatial resolution.

2.1 Sample Preparation

2.1.1 Fabrication of XAS specimen

XAS data of corroded alloy specimens must be collected in transmission mode. To achieve this, the specimen thickness is ideally 10-15 μm but not larger than 20 μm to allow for adequate transmission. We were able to purchase 10 μm foils of SS316 (MIT corporation) as well as foils of Inconel 625, (Installoy) but foils of Inconel 617 (INL, Progressive Alloy Steels Unlimited) will be fabricated from 1-inch plate material by cutting, grinding, and polishing.

2.1.2 Fabrication of diffusion specimen

Diffusivity of alloying metals in SS316, Inconel 625 and Inconel 617 will be determined from static ampoule type corrosion testing. The route of ampoule fabrication is sketched in the cartoon in Figure 21 applying the steps as following:

a) Tubes of Inconel 625, Inconel 617 and 316 will be welded at one end.

b) Foils of same metal (approx. 10mm × 10mm × 10μm) will be placed in bottom of tubes and filled with NaCl-$MgCl_2$

c) The tubes will be pinched shut at top and placed in quartz tubing.

d) The quartz tube will be vacuum sealed after 3 Ar backfill/vacuum cycles.

e) The quartz tubes will be placed in furnace.

f) Initial ramp 820 ℃ to melt salt.

g) Ramp down to target temperature.

h) Remove tubes after temperature holds.

i) The bottom of each tube will be sectioned off and sent to PNNL for analysis by XAFS

j) Remaining tube will be cut in cross-section and analyzed with SEM/EDS at UNLV

k) Imaging of corrosion effected zone, quantitative elemental profiling along the corrosion zone.

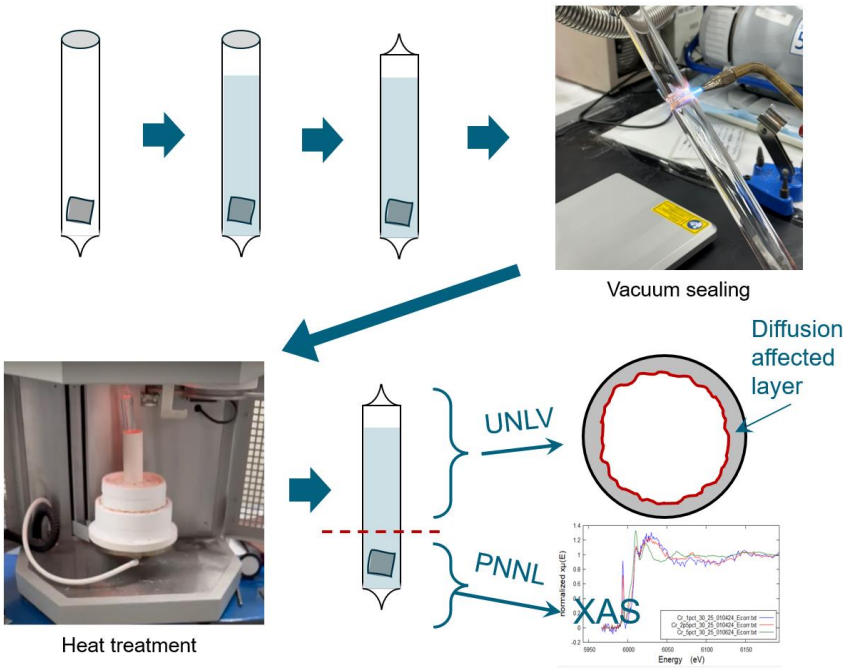

Figure 21. Fabrication of specimens to determine diffusivity and speciation

We have fabricated specimens of SS316 and IN 625 to determine diffusivity and speciation (Figure 22). Alloy foils with NaCl-$MgCl_2$ salt are sealed in SS316 and IN 625 ampoules, which are sealed on quartz tubes, to undergo heat treatment at 550 °C and 650 °C.

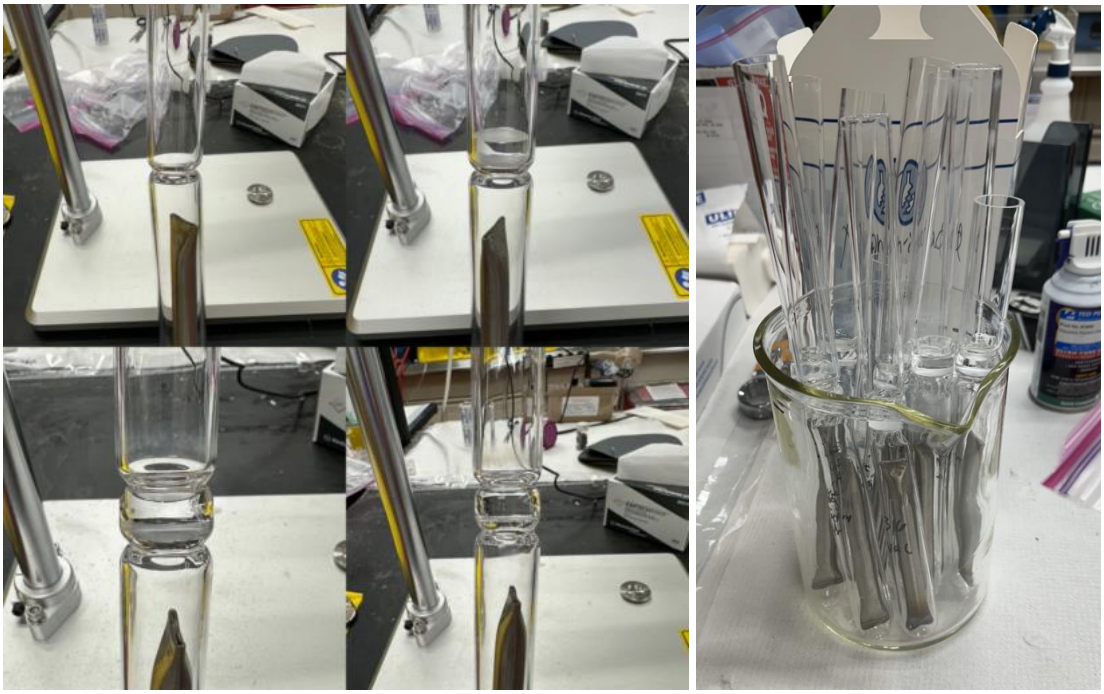

Figure 22. Diffusion specimens for subsequent heat treatment at 550 °C and 650 °C within three consecutive time intervals: 1, 3, and 9 months.

2.2 Analysis

2.2.1 X-ray Absorption Spectroscopy (XAS)

X-ray absorption spectroscopy (XAS) is performed using an *easy*XAFS300+ which has been fitted with a custom *in situ* and *in operando* cell, designed to heat to 800 °C and to operate with several different gases. The easyXAFS300 is designed to perform x-ray absorption fine structure (XAFS) and x-ray emission (XES) spectroscopies. These techniques provide details about the electronic states, bonding, and geometry of specific elements in molecules or materials. Previously this technology was only available at synchrotron beam lines. This benchtop instrument increases a researcher's ability to access XAFS and XES measurements as part of an integrated research workflow. This instrument can provide high-quality spectra with measurement times comparable to many synchrotron beamlines, with some spectra available in minutes, and operate at energy ranges best suited analyzing first row transition elements. Having two spectrometers allows one to be dedicated to XAFS and the other to XES measurements. XAFS spectroscopy uses the interference of electrons released by exciting the sample with x-rays to discern the geometry of the local atomic structure. XES monitors energy given off by the relaxation of electrons to probe the spin and oxidation state of ions, as well as help identify the ions or molecules that bind to the central metal atom and determine its reactivity (Figures 23 and 24).

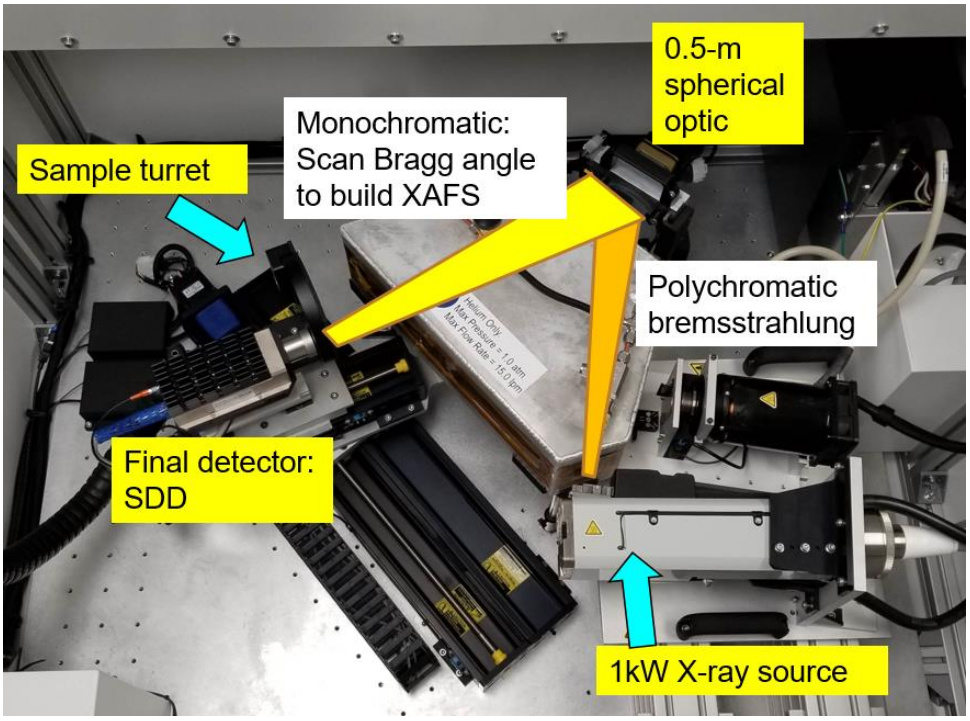

Figure 23. PNNL's EasyXAFS 300 for *in-situ* determination of corrosion species by XAFS measurements

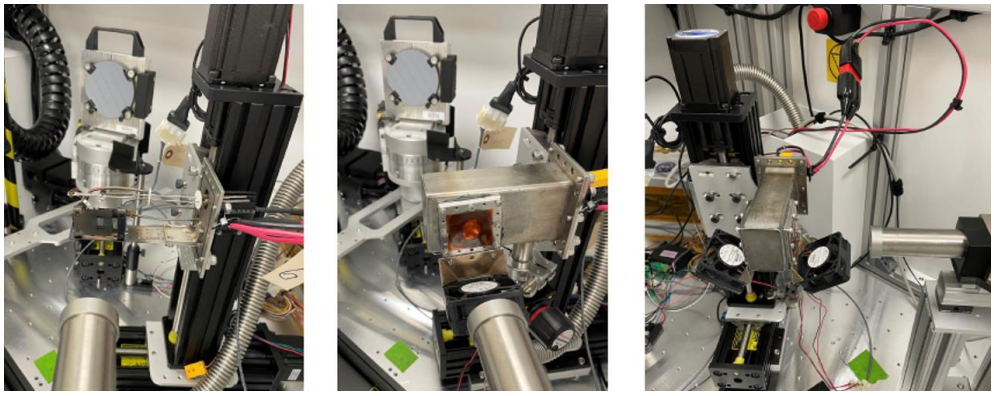

Figure 24. Inert vacuum furnace attachment to allow for in-situ X-ray absorption spectroscopy (XAS) under in-operando conditions

2.2.2 Speciation of metal-chloride corrosion products

2.2.2.1 Proof of Concept

Our experimental setup at PNNL will allow for speciation of corrosion products in transmission mode. As a proof of concept, 10 μm foils of Cr, Fe, and Ni have been purchased from the MIT corporation. XAS measurements before and after these foils have been exposed to molten chloride salts have been conducted (Figure 25). The measurements indicate different local environments of Cr, Fe, and Ni in the pure metal relative to the local environment in austenitic SS316. XAS can be therefore adapted to provide fine-structure information of metal foils and their alteration by the exposure to molten chloride salts.

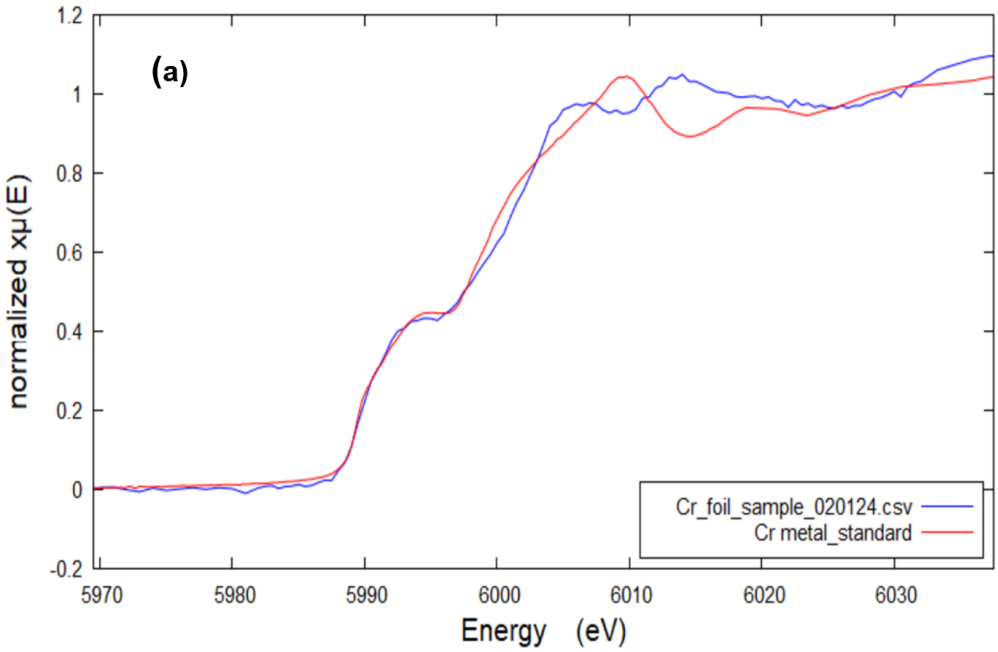

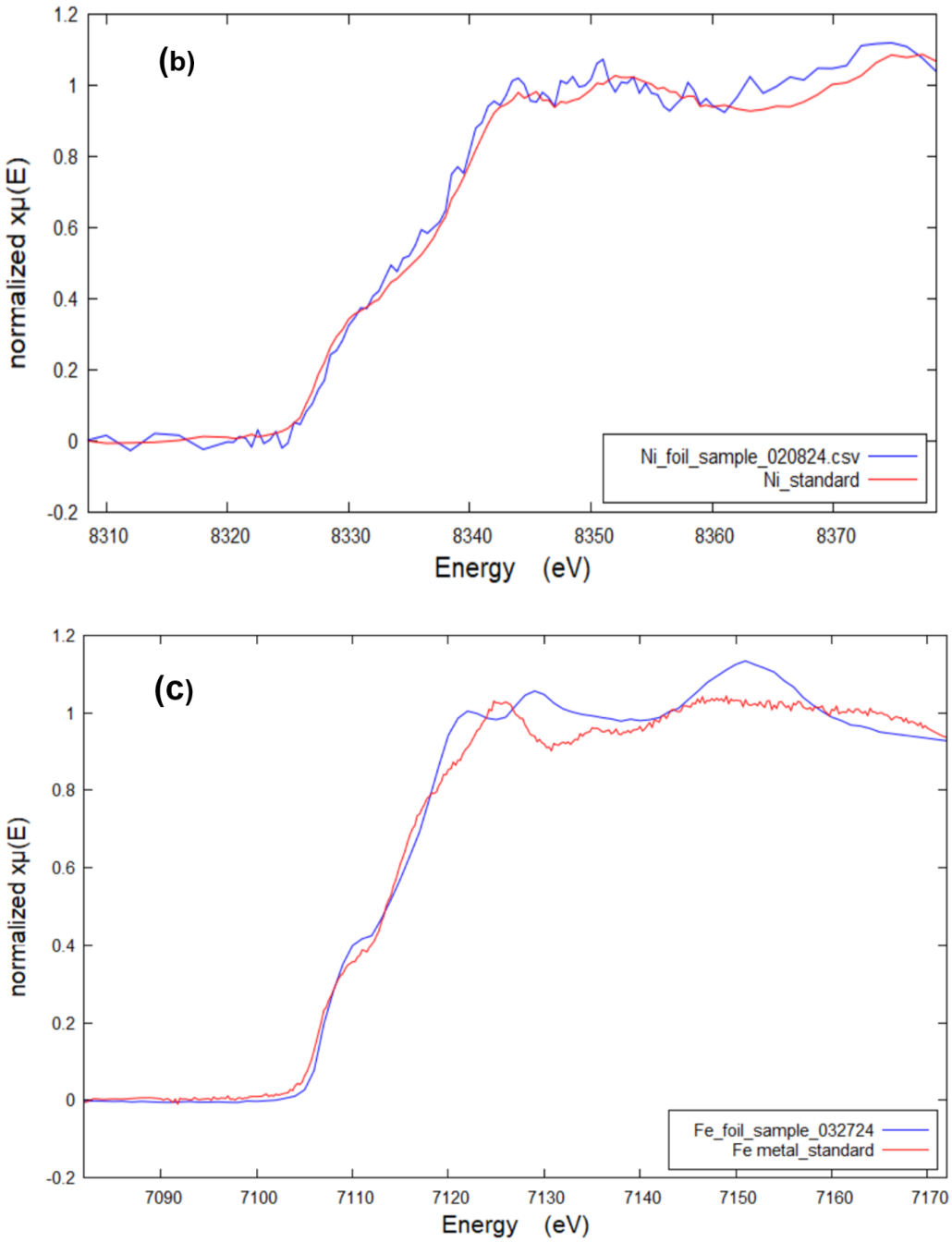

Figure 25. X-ray absorption spectra of corroded foils of chromium (a), nickel (b), and iron (c) compared with the pristine metal foils

At the interface of stainless steel with molten chloride salts chromium has been shown to be the most active alloying metal. Therefore, we fabricated mixtures of chromium powder (1, 2.5, and 5 wt.%) with eutectic Na-Mg chloride. XAS data show that at low chromium concentration Cr(VI) is the dominant species while at higher chromium concentration Cr(VI) and Cr(III) are present at equal concentrations (Figure 25).

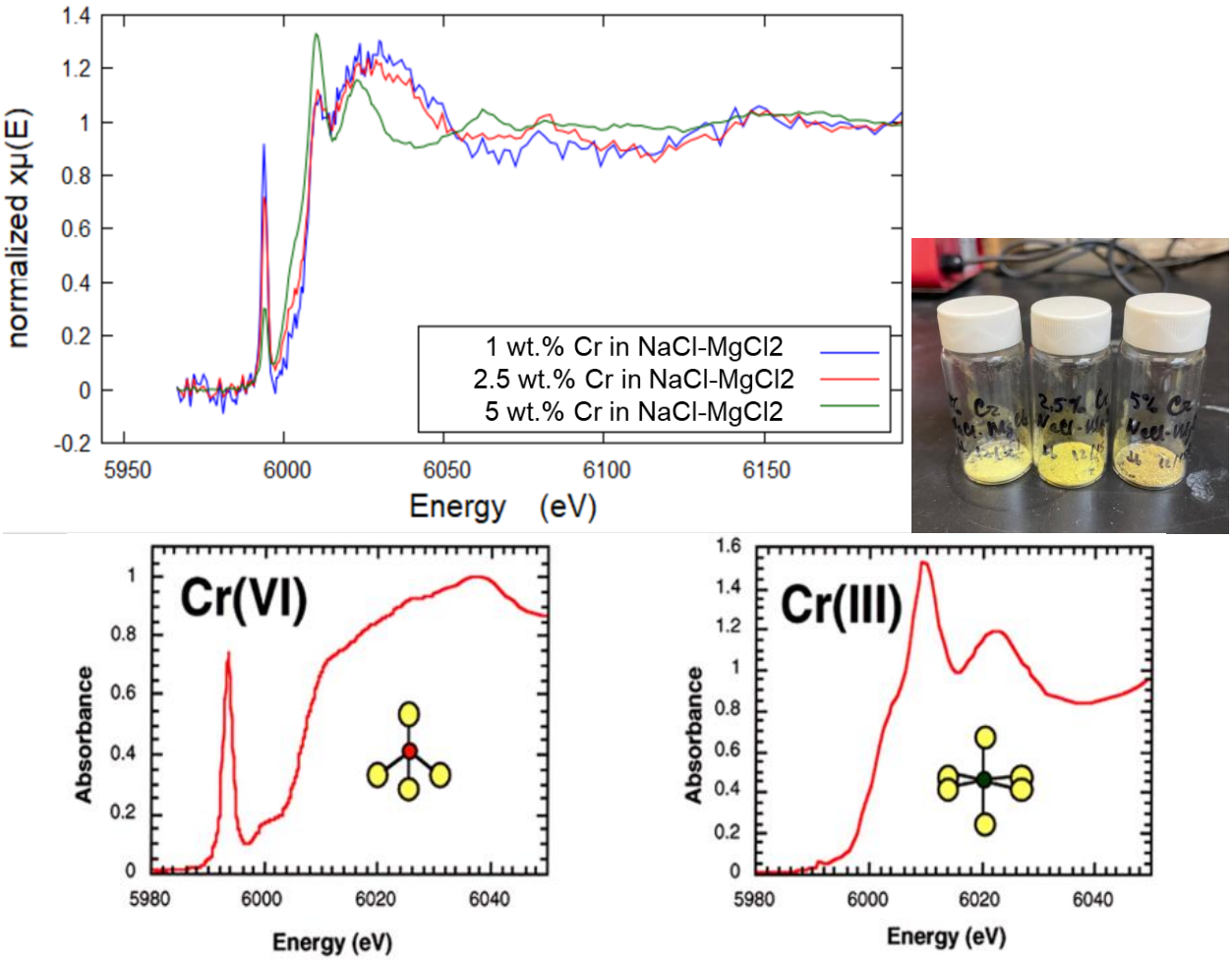

Figure 26. XAS of Cr-chlorides annealing 1, 2.5, and 5 wt.-% Cr in eutectic NaCl-$MgCl_2$

3.0 Outlook for FY2025

In FY2024 we have successfully established laboratory space to perform MSR-related corrosion studies to decipher diffusivity and speciation of corroded stainless-steel (S31600) and Inconel (IN 625, IN 617). Analysis using metallography and electron microscopy will be combined with x-ray absorption spectroscopy in a novel configuration. The experimental work scope at our university research partner UNLV is tuned to provide reproducible data on corrosion specimen ampoules. During the experiments any air contact of the eutectic Na-Mg-chloride salt must be always avoided, to allow for the collection of suitable data to represent prospective MSR *in-operando* conditions. We have established work protocols for use which capture the added complexity of and the addition of uranium chloride as well as fission products such as fission tellurium and fission lanthanides planned in FY2025 and beyond.

In FY2024 we could not deliver all data as promised, therefore corrosion testing on SS316 and Inconel 625 will continue most of FY2025 to collect significant data on the diffusivity of alloying metals at 550 °C and 650 °C in molten NaCl-$MgCl_2$. Furthermore, we will gain sufficient information on the speciation of the corrosion products as soon as the annealing of the metal foils comes to completion.

Our main focus on FY2025 is to gain knowledge on the corrosion behavior of Haynes 244 in molten NaCl-$MgCl_2$ and Na-Mg-U-chloride salt melts. The current data for Haynes 244 with respect to MSR deployment are insufficient and our aim is to start establishing a corrosion property data base for Haynes 244 in FY25. As discussed in section 1.7, Haynes 244 is a valuable candidate alloy for MSR. We plan to perform ampoule-type corrosion tests of Haynes 244 bulk material and foils in at 650 °C and 850 °C using the surrogate NaCl-$MgCl_2$ salt as well as the Na-U-Cl fuel salt with the addition of magnesium as reducing agent.

4.0 References

[1] K. Power, Kairos Power Begins Construction on Hermes Low-Power Demonstration Reactor. https://kairospower.com/media/.
[2] U.S. NRC, MSRR – Abilene Christian University Application. https://www.nrc.gov/reactors/non-power/new-facility-licensing/msrr-acu.html. (Accessed September 9 2024).
[3] U.S. NRC, Abilene Christian University Molten Salt Research Reactor Construction Permit 2024.
[4] P. Patel, China Says It's Closing in on Thorium Nuclear Reactor, IEEE Spectrum, 2021.
[5] V. Ignatiev, O. Feynberg, I. Gnidoi, A. Merzlyakov, V. Smirnov, A. Surenkov, I. Tretiakov, R. Zakirov, V. Afonichkin, A. Bovet, V. Subbotin, A. Panov, A. Toropov, A. Zherebtsov, Progress in Development of Li,Be,Na/F Molten Salt Actinide Recycler & Transmuter Concept, ICAPP 2007, Nice, France, 2007.
[6] V. Ignatiev, A. Surenkov, Material performance in Molten Salts, Elsevier2012.
[7] E.S. Bettis, R.W. Schroeder, G.A. Cristy, H.W. Savage, R.G. Affel, L.F. Hemphill, The Aircraft Reactor Experiment - Design and Construction, Nuclear Science and Engineering 2(6) (1957) 804-825.
[8] W.D. Manly, G.M. Adams, J.H. DeVan, D.A. Douglas, E.E. Hoffman, P. Patriarca, Aircraft reactor experiment – metallurgical aspects, Oak Ridge National Lboratory, 1957, p. 59.
[9] W.D. Manly, J.H. Coobs, J.H. DeVan, Metallurgical problems in molten fluoride systems, Prog. Nucl. Energy 2(4) (1960).
[10] J.H. DeVan, R.B. Evans, Corrosion Behavior of Reactor Materials in Fluoride Salt Mixtures, Oak Ridge National Laboratory, 1962, pp. 1-39.
[11] J.R. DiStefano, J.H. DeVan, J.R. Keiser, R.L. Klueh, W.P. Eathery, Materials Consideration for Molten Salt Accelerator-based Plutonium Conversion Systems, Oak Ridge National Laboratory, 1995.
[12] E. Industries, The Molten Chloride Salt Fast Reactor, 2020. http://www.elysiumindustries.com/technology.
[13] T. LLC, TerraPower's Molten Chloride Fast Reactor Technology: Retooling for a Changing Energy Sector, 2020. http://www.terrapower.com.
[14] M. Energy, Stable Salt Reactors, 2020. https://www.moltexenergy.com/stablesaltreactors/.
[15] D.E. Holcomb, G.F. Flanagan, B.W. Patton, J.C. Gehin, R.L. Howard, T.J. Harrison, Fast spectrum molten salt reactor options, 2011, p. 33.
[16] S. Guo, J. Zhang, W. Wu, W. Zhou, Corrosion in the molten fluoride and chloride salts and materials development for nuclear applications, Progress in Materials Science 97 (2018) 448-487.
[17] P. Chartrand, A.D. Pelton, Thermodynamic Evaluation and Optimization of the LiCl-NaCl-KCl-RbCl-CsCl-MgCl2-CaCl2 System Using the Modified Quasi-chemical Model, Metallurgical and Materials Transactions B 32 (2001) 1361-1383.
[18] T. Hartmann, P. Paviet, Corrosion of Containment Alloys in Molten Salt Reactors and the Prospect of Online Monitoring, JNFCWT 20(1) (2022) 43-63.
[19] R. Tewari, N.K. Sarkar, D. Harish, B. Vishwanadh, G.K. Dey, S. Banerjee, Intermetallics and Alloys of High Temperature Application, Materials under Extreme Conditions, Elsevier2017, pp. 293-335.
[20] R. R., Z. Anorg. Chem 117 (1921).
[21] M. Corum J, B. J.J., Rules for design of alloy 617 nuclear component to very high temperatures, American Society of Mechanical Engineers (ASME) pressure vessels and piping conferenc, Oak Ridge National Laboratory, San Diego, CA, 1991.

[22] K. J., Alloy 617 and derivates, Materials for Ultra-Supercritical and Advanced Ultra-Supercritical Power Plants, Woodhead Publishing2017, pp. 547-570.
[23] H. Kirchhoefer, J. Rottmann, F. Schubert, H. Nickel, Untersuchungen zum isothermen Ausscheidungsverhalten von Nickelbasislegierungen mit Hilfe der elektrochemischen Phasenisolierung, Berichte der Kernforschungsanlage Juelich, Kernforschungsanlage Juelich, 1984, p. 128.
[24] G. Maier, Microstructure, deformation and lifetime of Alloy 617B. Experiments, models and component predictions; Mikrostruktur, Verformung und Lebensdauer der Legierung Alloy 617B. Experimente, Modelle und Bauteilvorhersagen, Karlsruhe Institut fuer Technologie (KIT), 20132, p. 170.
[25] H.v. Wortel, Control Of Relaxation Cracking In Austenitic High Temperature Components, Corrosion 2007, Nashville, TN, USA, 2007.
[26] D. Tytko, P.-P. Choi, J. Kloewer, A. Kostka, G. Inden, D. Raabe, Microstructural evolution of a Ni-based superalloy (617B) at 700 C studied by electron microscopy and atom probe tomography, Acta Materialia 60 (2012) 1731-1740.
[27] A. Talukder, P.J. Felfer, M. Chaturvedi, L.T. Stephanson, M.R. Kilburn, J.M. Cairney, Segregation of B, P, and C in the Ni-Based Superalloy, Inconel 718, Metallurgical and Materials Transactions A 43(July 2012) (2012) 2183-2191.
[28] H.A. Roth, C.L. Davis, R.C. Thomson, Modeling Solid Solution Strengthening in Nickel Alloys, Metallurgical and Materials Transactions 28A (1997) 1329-1665.
[29] M.G. Fahrmann, J.R. Crum, Formation of Pt2Mo type phase in long-term aged Inconel Alloy 686 Superalloys 2000, The Minerals, Metals & Materials Society (TMS), 2000, pp. 813-820.
[30] H.C. Pai, M. Sundararaman, B.C. Maji, A. Biswas, M. Kirshnan, Influence of Mo addition on the solvus temperature of Ni2(Cr,Mo) phase in Ni2(Cr,Mo) alloys, Journa of Alloys and Compounds 491 (2010) 159-164.
[31] J.W. Koger, Alloy compatibility with LiF-BeF2 salts containing ThF4 and UF4, 1972, p. 43.
[32] V. Ignatiev, A. Surenkov, Alloys compatibility in molten salt fluorides: Kurchatov Institute related experience, J. Nucl. Mater. 441(1-3) (2013) 592-603.
[33] W. Ren, Considering of Alloy N Code Extension for Commercial Molten Salt Reactor Development and Deployment, Proceedings of the ASME 2018, Prague, Czech Repoblic, 2018.
[34] J.A. Lane, H.G. MacPherson, F. Maslan, Fluid fuel reactors, Addison-Wesley Publishing Co, Massachusetts, 1958.
[35] H. International, Haynes 244 Alloy.
[36] H. International, Haynes 230 alloy, Haynes International 2021, p. 29.
[37] H. International, Haynes 188 alloy, in: H. International (Ed.) 2018, p. 18.
[38] H. International, Haynes 214 alloy, in: H. International (Ed.) 2021, p. 28.

Pacific Northwest National Laboratory

902 Battelle Boulevard
P.O. Box 999
Richland, WA 99354

1-888-375-PNNL (7665)

www.pnnl.gov